ATP synthase K^+- and H^+-flux drive ATP synthesis and enable mitochondrial K^+-uniporter function

Magdalena Juhaszova,[1,9] Evgeny Kobrinsky,[1,9] Dmitry B. Zorov,[1,5,9] H. Bradley Nuss,[1†] Yael Yaniv,[1‡] Kenneth W. Fishbein,[2] Rafael de Cabo,[3] Lluis Montoliu,[6] Sandra B. Gabelli,[4,7,8] Miguel A. Aon,[1] Sonia Cortassa,[1] and Steven J. Sollott[1,*]

[1]Laboratories of Cardiovascular Science and [2]Clinical Investigation, and [3]Translational Gerontology Branch, National Institute on Aging, NIH, and [4]Dept. Medicine, [7]Dept. Oncology, [8]Dept. Biophysics and Biophysical Chemistry, Johns Hopkins University School of Medicine, Baltimore, MD, USA
[5]A.N. Belozersky Institute of Physico-Chemical Biology, Lomonosov Moscow State University, Moscow, Russia
[6]Centro Nacional de Biotecnología, CSIC, Madrid, Spain

Present address:
[†]Center for Scientific Review, NIH, Bethesda, MD, USA
[‡]Biomedical Engineering Faculty, Technion-IIT, Haifa, Israel

[9] Co-first author

* Corresponding author. Tel: +1 410 558 8657; Fax: +1 410 558 8150; E-mail: sollotts@mail.nih.gov

Running title: ATP synthase K^+- and H^+-flux drive ATP synthesis

Corresponding author:
Steven J. Sollott, M.D.
Chief, Cardioprotection Section
Laboratory of Cardiovascular Science
Biomedical Research Center, Suite 100
National Institute on Aging, NIH
251 Bayview Blvd
Baltimore, MD 21224-2816
USA

Abstract

We show that mammalian ATP synthase (F_1F_o) utilizes the ion gradient energy not only of H^+ but also of K^+ to make ATP with the relative permeability of H^+:K^+ at ~10^6:1. F_1F_o can be upregulated to increase the total ion-flux (at constant H^+:K^+) against a constant load without slip or leak, via the IF_1-mediated increase in chemo-mechanical efficiency of F_1F_o regulated by endogenous survival-related proteins, Bcl-xL and Mcl-1, and synthetic small molecules, diazoxide and pinacidil. Increasing ATP synthesis driven by K^+- and H^+-influx through F_o provides a simple way for F_1F_o to operate as a primary mitochondrial K^+-uniporter to regulate matrix osmotic balance matching metabolic energy supply with demand. This essential mitochondrial homeostatic mechanism also enables F_1F_o to function as a recruitable mitochondrial K_{ATP}-channel, whereby triggered increases of mitochondrial K^+-influx and matrix-volume upregulate the signal cascade resulting in desensitization of the permeability transition pore, enhancing cell survival during ischemia-reperfusion injury.

Keywords

ATP synthase regulation / ATPase Inhibitory Factor-1 (IF_1) / Bcl-2 family proteins / mitochondrial potassium transport and volume regulation / mitochondrial permeability transition pore

Introduction

The family of ATPases shares a number of proteins with conserved functions and molecular composition (Cross & Muller, 2004). F-, A- and V-ATPases are true biological rotary engines that work as coupled motors: the $F_1/A_1/V_1$ is chemically driven (i.e., effecting transduction of mechanical and chemical energy) and the membrane-embedded $F_o/A_o/V_o$ is powered by the energy stored in a transmembrane ion gradient (Kuhlbrandt & Davies, 2016; Stock et al, 1999). Of these, a specialized group, the ATP *synthases*, is the major route to ATP synthesis. One of the best characterized members of ATPases is the F_1F_o-ATP synthase (F_1F_o) of E. coli, mitochondria and chloroplasts. It was demonstrated that both F_1 and F_o subunits are required for ATP synthesis (Boyer, 1997).

Most ATPases harness the free energy of the transmembrane electrochemical proton gradient, $\Delta\mu_H$, but some use a Na^+ gradient instead (e.g., see (Kaim & Dimroth, 1995)). Differences in amino acid (AA) composition may govern cation specificities. Double mutation in subunit c of the F_o moiety of the F_1F_o of *P. modestum* causes a switch from Na^+- to H^+-coupled ATP synthesis (Kaim et al, 1997). Reconstituted bovine F_o alone, although normally selective for H^+ in the intact F_1F_o complex, could form a K^+ channel (Miedema et al, 1994), suggesting that key determinants of ion selectivity could also be conferred by the interaction of F_o with the F_1 components.

ATP synthase operates as two rotary stepper generators coupled by a common shaft, the γ subunit (Abrahams et al, 1994; Boyer, 1997; Noji et al, 1997). The torque that is generated by ion flow through the F_o motor operates against the counter-torque in F_1 driven by the energy of ATP hydrolysis. The *direction* of F_1F_o is determined by which torque is larger: that of the driving force of the ion gradient or that produced by the ATP chemical potential. Under physiological conditions, F_o torque exceeds the F_1-generated counter-torque at ambient ATP levels, and thus the system proceeds toward ATP synthesis. Although the principal function of the F_1F_o is to harness the energy stored in electrochemical ion gradients to make ATP, it can nevertheless run backwards (as an ATP hydrolase) pumping ions in the opposite direction in the absence of the activity of a regulated inhibitory protein. This scenario would occur if, (1) the ATP levels would rise substantially relative to the ion gradient magnitude, or (2) the ion gradient becomes dissipated, as occurs during ischemia.

During ischemia, consuming substantial amounts of ATP at a time when its supply is limited would likely be detrimental in energetically-sensitive cells such as cardiomyocytes and neurons. It is known that Inhibitory Factor-1 (IF_1), a small ~12kDa regulatory protein, limits the reversal of F_1F_o function, and that during ischemia this helps to prevent excessive (or even futile) ATP consumption by damaged mitochondria to maintain $\Delta\Psi_m$. Opening of an ATP-inhibited mitochondrial K^+ channel (mK_{ATP}), activated either by repetitive short periods of ischemia ("ischemic preconditioning") or by K^+ channel openers (KCO) such as diazoxide (Dz), serves as a critical link in a cascade of kinases preventing the deleterious effects of opening the mitochondrial permeability transition pore (mPTP), limiting cell damage and death after ischemia (Juhaszova et al, 2008; Juhaszova et al, 2004; Zorov et al, 2009). Interestingly, Dz binds to and enhances the inhibitory functions of IF_1 (Contessi et al, 2004) suggesting a tendency to preserve ATP during ischemia that may lead to enhanced cell survival and resistance to damage.

While the mechanistic basis of ion-selectivity of various ATP synthases is a matter of considerable interest (Leone et al, 2015), it is even more intriguing to consider the possible significance for mitochondrial function of the accompanying "*non*-specific" ion flux via F_1F_o. The specificity of F_1F_o for H^+ over other cationic species was found to be extremely high (estimated $>10^7$) (Feniouk et al, 2004). It can be calculated using the Goldman-Hodgkin-Katz equation (Hille, 2001) that for H^+ selectivity values of 10^7 and 10^8, F_1F_o would conduct a non-trivial ~24 and 2 K^+, respectively, for every 100 H^+ during normal ATP synthesis (at cytosolic pH=7.2 and K^+=140 mEq/L) due to the $>10^6$-fold excess of cytoplasmic K^+ over H^+. Given the large electrical force driving K^+ to the mitochondrial matrix, it would make sense to harness this energy to generate ATP rather than to dissipate $\Delta\mu_K$ as heat. Because the activity of the respiratory chain is known to be regulated by intramitochondrial volume controlled by K^+ influx (Garlid et al, 2003), the added benefit would be the direct coupling of respiratory chain activity and $\Delta\Psi_m$ dissipation (caused by energy utilization/production) to an osmotic signal given by the amount of K^+ traversing F_1F_o to make ATP, facilitating the proportional matching between energy supply and demand. Finally, that part of the proton gradient and energy not being directly dissipated via ATP synthase because of the equivalent movement of charge as K^+ would then be available to drive K^+ efflux from mitochondria using the K^+/H^+ exchanger (KHE), thus restoring osmotic balance. These principles are fully compatible with Mitchell's chemiosmotic mechanism (Mitchell, 1961; Nicholls & Ferguson, 2013).

We investigated the possible existence of a novel, regulated function set for ATP synthase based on the postulated ability to harness energy from K^+ flux. This would enable K^+ uniporter-like function and serve to facilitate energy supply-demand matching, while under certain circumstances, also to function as a mK_{ATP}. We found that while retaining the high degree of H^+-selectivity, the chemo-mechanical efficiency, and the monovalent cation conductance of F_1F_o can be increased by certain KCOs and by endogenous pro-survival proteins, Bcl-xL and Mcl-1. This process requires IF_1, and is regulated naturally by the concentration of ATP. We also demonstrated its role in protection signaling in intact cardiomyocytes.

Results

Potassium channel openers activate K^+ flux into proteoliposome-reconstituted ATP synthase

First, to measure K^+ flux into proteoliposome (PL)-reconstituted F_1F_o (see Figure 1-supplementary figure 1), the K^+-sensitive fluorescent dye, PBFI, was trapped inside the vesicles under conditions shown in Figure 1A. In the presence of the protonophore FCCP (to enable charge balance necessary for K^+ flux and to maintain $\Delta\Psi_m$=0), the K^+ channel opener (KCO) diazoxide (Dz) significantly enhanced the initial rate of K^+ flux into PL; this effect was completely blocked both by the F_o inhibitor venturicidin B (Vent), and the mK_{ATP} blocker, 5-hydroxydecanoate (5-HD), while it was essentially absent in IF_1-depleted F_1F_o (Figure 1B).

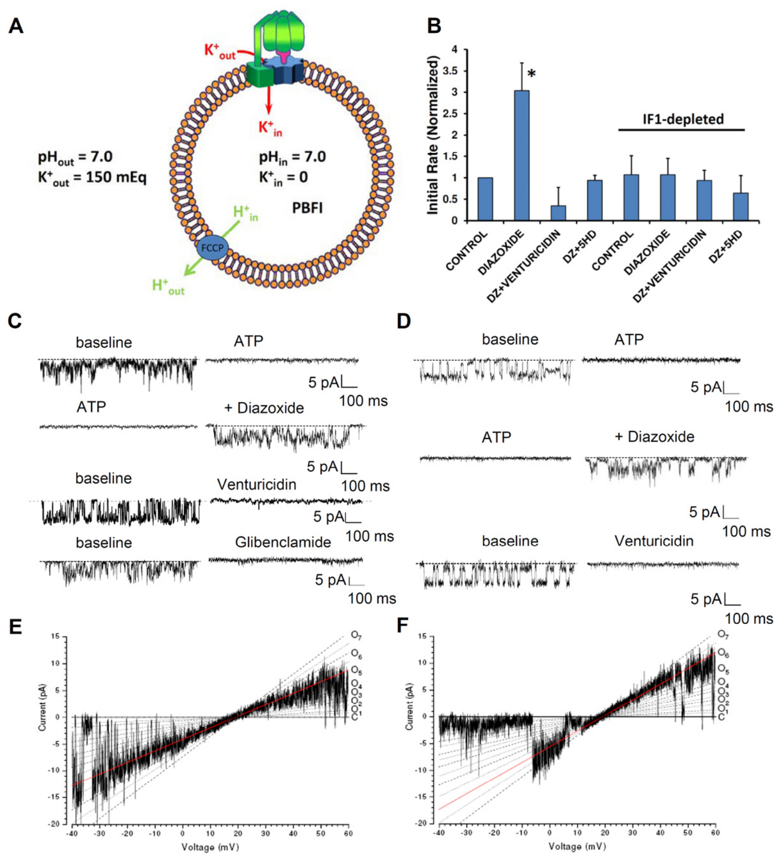

Figure 1. Characterization of K^+ fluxes through purified, reconstituted F_1F_o. (**A**) Scheme of the proteoliposome (PL) system; ionic composition of the internal and external buffer, used in K^+ transport experiments. (**B**) Kinetics of K^+ flux into PL; effect of IF_1 depletion. The potassium channel opener (KCO), diazoxide (Dz), significantly enhanced the kinetics (i.e., rate) of K^+ flux into PL; this effect was blocked both by the F_o inhibitor, Vent, and the mK_{ATP} blocker, 5-HD, and was absent in IF_1-depleted F_1F_o. * $P<0.05$. Planar lipid bilayer experiments. (**C**) Unitary K^+ currents from purified F_1F_o (at -20 mV), and (**D**) from conventional mitochondrial membrane preparation (at -40 mV), reconstituted into lipid bilayers; pre-intervention baseline recordings are on the left, and the effect of the various compounds are shown (1 mM MgATP, 30 μM Dz, 4 μM Vent, 50 μM Glib). KCOs reverse ATP-inhibited permeation of F_1F_o by K^+ that can be blocked by Vent and Glib. (**E,F**) Unitary K^+ currents elicited in response to a voltage ramp (14.1 mV/sec) distinguish multiple conductance levels O_1-O_7 (panel **E-F**). The 216 pS conductance (O_5) is predominately active in the recording shown in panel **E**, while the 293 pS conductance (O_6) is active during the recording in panel **F**.

Measurement of unitary K^+ and H^+ currents from F_1F_o

In unitary ion channel recordings from lipid-bilayer reconstitution experiments with purified F_1F_o, Dz reversed ATP-inhibited ion flux that can be blocked by the F_o inhibitor, Vent, by the mK_{ATP} inhibitor, glibenclamide (Figure 1C) and by F_o inhibitors oligomycin and *N,N'*-dicyclohexylcarbodiimide (DCCD; not shown). Considering that similar findings are obtained in conventional mitochondrial membrane reconstitution studies (i.e., without using a purified F_1F_o), for the first time we show that the unitary ion currents derived from conventional mK_{ATP} preparations, which display the same characteristics as the purified F_1F_o complex, can be largely inhibited by Vent (Figure 1D) at levels that do not affect sarcolemmal mK_{ATP} currents. Unitary currents from purified F_1F_o exhibit multiple conductance levels (Figure 1E,F) in agreement with single channel behavior of conventional mK_{ATP} preparations. This complex behavior may arise from the multiple ion-binding positions on the F_o c-ring, the complete analysis of which is beyond the scope of the present report. A comprehensive literature search regarding the single channel characteristics of conventional mKATP channel preparations reconstituted into lipid bilayers indicates that multiple levels are frequently observed (five distinct peaks/conducting states between 20 pS and 120 pS in symmetric 150 mM K glutamate (Jiang et al, 2006; Nakae et al, 2003) and conductances between 100-275 pS in symmetric 100 mM KCl (Grigoriev et al, 1999; Mironova et al, 1999) which is largely consistent with the present data.

The ion-specificity of the observed unitary currents requires closer examination because mammalian F_1F_o is thought to make ATP only by H^+ flux. In the present experiments, the abundance of K^+ over H^+ was ~10^6:1 (comparable to that occurring in cells), so it is reasonable to consider that K^+ permeation may be contributing as well. Furthermore, the potential contribution of anion permeation cannot be excluded *a priori*. Because only permeant ions contribute to the net ion-current reversal potential (E_{rev}), this was examined in detail under various conditions to assess the possibility of anion permeation and to interpret the changes in cation permeation activated by KCOs. Since complete substitution of the substantially larger and rather non-permeant Hepes anion for Cl^- causes no change in E_{rev} (17.9 ± 0.7 vs 18.6 ± 0.5 mV, respectively, *P*=ns), we concluded that the impact of Cl^- permeation via F_1F_o is insignificant compared to cations. Additionally, the current-voltage relationship of purified F_1F_o was examined in a pH gradient (pH_{cis}=8.0, pH_{trans}=7.2, buffered by TEA^+-Hepes, in the absence of K^+ or any other small cation aside from H^+) yielding a reversal potential identical to the expected Nernst potential for H^+ as the only permeant species, in agreement with the idea that the OH^- anion is non-permeant. Since the measured unitary ion currents under control conditions consist only of H^+ and K^+, we next assessed their relative contributions. Under ionic conditions where the reversal potential for H^+ (E_H) was 0 mV and that for K^+ (E_K) was +28 mV, E_{rev} was found to be ~+18 mV indicating that both cations must be permeant and contributing to the total currents observed. In this case, E_{rev} is given by:

$$E_{rev} = \frac{RT}{F}\ln\left(\frac{P_K[K]_o + P_H[H]_o}{P_K[K]_i + P_H[H]_i}\right) = \frac{RT}{F}\ln\left(\frac{[K]_o + \frac{P_H}{P_K}[H]_o}{[K]_i + \frac{P_H}{P_K}[H]_i}\right) \quad (1)$$

where:

R is the molar gas constant

F is Faraday's constant

T is temperature (°K)

P_K and P_H are the respective ion permeabilities

$[K]_{o,i}$ and $[H]_{o,i}$ are ion concentrations across the bilayer

Maintaining steady voltages at each of the ion-reversal potentials (to remove the driving force from the specific cation, thus rendering pure unitary current from the other cation) produced macroscopic H^+ and K^+ currents (at +28 and 0 mV, respectively) of the same characteristics and open probability (P_o) as at -20 or -40 mV (Figure 1E,F). Importantly, the KCO Dz increases P_o and amplitude for both H^+ and K^+ currents (Figure 1C,D) without causing any change in E_{rev} (18.3 ± 1.3 vs 18.5 ± 0.9 mV with Dz, P=ns; similar data was obtained with Na^+: 18.1 ± 1.0 vs 18.9 ± 1.0 mV). This indicates that while the permeability for H^+ and K^+ after Dz increases for both cations, the ratio (P_H/P_K) remains unchanged (see eq.1). From the Goldman-Hodgkin-Katz (GHK) formalism, the total ion current is related to the individual ion permeability as follows:

$$I = P_H Z_H^2 \frac{VF^2}{RT}\left(\frac{[H]_i - [H]_0 \exp\left(\frac{-Z_H VF}{RT}\right)}{1-\exp\left(\frac{-Z_H VF}{RT}\right)}\right) + P_K Z_K^2 \frac{VF^2}{RT}\left(\frac{[K]_i - [K]_0 \exp\left(\frac{-Z_K VF}{RT}\right)}{1-\exp\left(\frac{-Z_K VF}{RT}\right)}\right) \quad (2)$$

where:

Z is the appropriate ion valence

V is the transmembrane voltage

We determined that the baseline values for P_H and P_K (5.2±0.9 $\times 10^{-11}$ and 8.7±2.9 $\times 10^{-17}$ m^3/s, respectively) each increases ~3.5-fold after Dz (to 2.2±1.3 $\times 10^{-10}$ and 3.0±1.4 $\times 10^{-16}$ m^3/s, respectively, n=4, both $P<0.05$ *vs.* each ion's baseline value), thus keeping the selectivity of F_1F_o for H^+ over K^+ at ~10^6:1. Regarding the single ion channel behavior of the conventionally-prepared mK_{ATP}, close inspection of the electrophysiological data referred in eight published papers allowed us to extract baseline values for P_H and P_K (mean values of 4.9±1.1 $\times 10^{-11}$ and 1.9±0.5 $\times 10^{-16}$ m^3/s, respectively) (Bednarczyk et al, 2005; Dahlem et al, 2004; Grigoriev et al, 1999; Jiang et al, 2006; Mironova et al, 1981; Mironova et al, 2004; Nakae et al, 2003; Zhang et al, 2001) which compare extremely well with those obtained here for F_1F_o.

The importance of F_1F_o as a major K^+ pathway can be realized from Eq. 2 which shows the sum of the K^+ and H^+ current components in the GHK formulation. For sufficiently large $\Delta\Psi_m$ magnitudes (>100 mV for the present case), a rearrangement of Eq. 2 expressing the ratio of K^+ to H^+ conducted by F_1F_o simplifies to the limiting value, $[(P_K \cdot [K^+]_{cytosol})/(P_H \cdot [H^+]_{cytosol})]$ at *negative*

$\Delta\Psi_m$ (the direction of ATP *synthesis*). This means that F_1F_o may potentially conduct an average of 3.7 K^+ for every H^+ during *normal* ATP synthesis (at cytosolic pH=7.2 and K^+=140 mEq/L; see Supplementary file 1).

Using an electrophysiological approach, we ruled out the presence of any other cation-selective channel activity in our F_1F_o preparations (Figure 1 – figure supplement 2A,B). It has been suggested that a mitochondrial ROMK potassium channel might act as the pore-forming subunit of a cytoprotective mK_{ATP} channel (Foster et al, 2012). Our immunoblotting with anti-ROMK antibody ruled out ROMK channel contamination of the isolated F_1F_o (Figure 1 – figure supplement 2C).

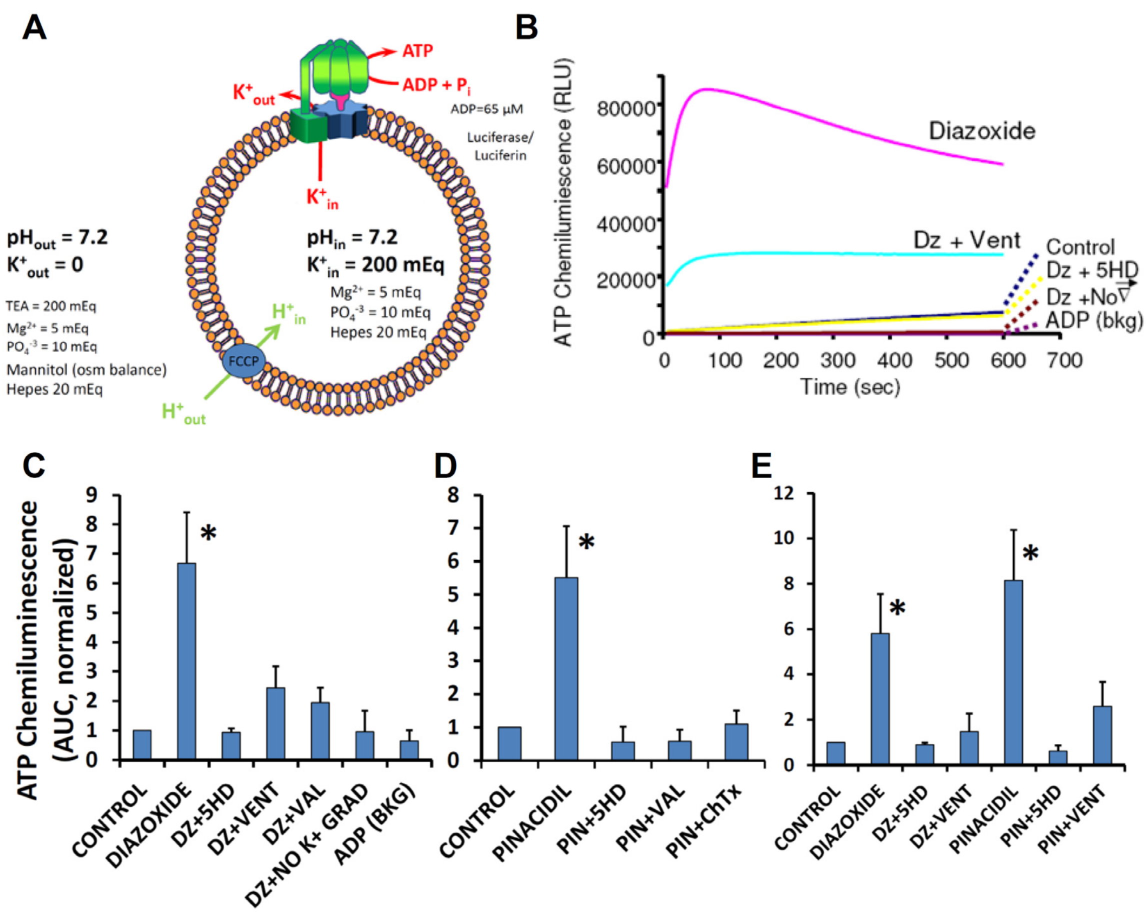

Figure 2. ATP synthesis afforded by K^+ flux through reconstituted F_1F_o. (**A**) Scheme of the PL and reaction conditions to measure K^+ transport-coupled ATP synthesis (and hydrolysis). $\Delta\mu_H$=0 for ATP synthesis and $\Delta\Psi$=0 by using FCCP; n.b., omitting FCCP eliminates ATP synthesis ruling out the presence of an unsuspected, underlying K^+/H^+ antiport mechanism. (**B,C**) K^+-gradient-driven ATP production in PL is activated by Dz and (**D**) pinacidil, and (**B-D**) attenuated by inhibitors of F_1F_o (Vent), inhibitors of the mK_{ATP} (5HD) and BK_{Ca} channels charybdotoxin (ChTx), and by K^+ gradient dissipation (Val or No K^+ grad). (**E**) Na^+-gradient-driven ATP production in PL is activated by Dz and pinacidil and attenuated by inhibitors of F_1F_o and the mK_{ATP}. These experiments prove that the entity activated by KCOs is the F_1F_o. * $P<0.05$.

ATP synthesis by proteoliposome-reconstituted F_1F_o in a K^+ gradient

To investigate whether ATP synthase can harness energy from K^+-flux, purified F_1F_o reconstituted into PL was subjected to a transmembrane K^+ gradient (Figure 2A). Under conditions in which $\Delta\Psi=0$, and $\Delta\mu_H$ and H^+ were unable to drive ATP synthesis due to the presence of protonophore, FCCP, we show that ATP synthesis occurs under these conditions, and was increased several-fold by the KCOs, Dz or pinacidil. This ATP synthesis was inhibited by the specific F_o inhibitor, Vent, the mK_{ATP} blocker, 5-HD, and abolished by the K^+ ionophore, valinomycin (Figure 2B-D). It is important to note that FCCP is used here to enable ATP synthesis by the K^+ gradient by equilibrating the transmembrane charge (via passive inward diffusion of H^+) owing to gradient-driven K^+ efflux via F_1F_o. Omitting FCCP eliminates ATP synthesis ruling out the possible contamination of the PL's by an unsuspected protein which might cause an underlying K^+/H^+ antiport activity (see Figure 1 – figure supplement 2 for additional details). Any possibility that the observed ATP synthesis was due to F_1F_o surreptitiously harnessing H^+ flux energy (somehow derived from the original K^+ gradient energy) is ruled out by this FCCP result, because ATP synthesis would instead have been prevented by the protonophore-elicited dissipation of H^+ energy. That ATP can be synthesized from a K^+ gradient (when H^+ is unable to drive ATP synthesis) indicates that it is the free energy of the ion gradient (i.e., $\Delta\mu_K$ but not $\Delta\mu_H$ or the counterions) and specifically the flux of K^+ that is harnessed by F_1F_o. This evidence also demonstrates that K^+ can drive ATP synthesis by the same mechanism and path as H^+. Interestingly, the F_1F_o is not selective among alkali ions after KCO-activation, since we observed a comparable degree of ATP synthesis in a Na^+ gradient, akin to that in a similar K^+ gradient (Figure 2E). Moreover, this effect seems to be restricted to small cations, since there is no ATP generated by KCO activation of the F_1F_o in a comparable gradient of TEA^+Cl^-. Similar K^+ gradients with either Cl^- or SO_4^{2-} as counterions yielded comparable ATP amounts. This also rules out that KCO-activated transmembrane K^+ (or Na^+) flux occurs via some unforeseen contaminating protein (see Figure 1 – figure supplement 2). We conclude that, in the presence of KCOs, F_1F_o becomes proportionately more permeant to H^+ and K^+ (while retaining the ~10^6:1 H^+ selectivity) – enabling measurably increased electrochemical gradient-driven permeation by K^+ to function as a mitochondrial ATP-dependent K^+ channel.

Together, the data presented indicate that K^+ flux-driven ATP synthesis can proceed with PL-reconstituted purified F_1F_o in addition to that normally achieved directly by the flux of a H^+ gradient. This is a remarkable and important new finding because mammalian F_1F_o is thought to make ATP only by H^+ flux. Such behavior also indicates that F_1F_o can potentially serve as a mitochondrial inner membrane K^+ channel. Additionally, in the presence of KCOs F_1F_o becomes proportionally more permeant to K^+ ions suggesting the possibility that it may function as a mitochondrial ATP-dependent K^+ channel (mK_{ATP}) by enabling measurably increased electrochemical gradient-driven permeation by K^+. In the following sections, we will measure and quantify the importance of these mechanisms.

We provide additional evidence from experiments in living cells to support the discovery that F_1F_o can function as a mK_{ATP}. Based on previous work by our group (Juhaszova et al, 2004; Juhaszova et al, 2009) as well as by others (Garlid et al, 2003; Halestrap, 1989; Sato et al, 1998) the following reveal key manifestations of mK_{ATP} activation in cardiomyocytes in response to KCOs: (1) flavoprotein (FP) oxidation, (2) modulation of mitochondrial regulatory swelling (i.e., due to mitochondrial K^+ accumulation), (3) volume activation of respiration (as a consequence of #2), (4) inhibition of GSK-3β activity via ser-9 phosphorylation, and (5) increased mPTP reactive oxygen species (ROS)-threshold. We examined each one of these manifestations of mK_{ATP} activation by Dz in myocytes with IF_1 knocked down by ~75% through gene silencing (Figure 3A-C), compared to cells treated with control siRNA (Figure 3A,B). Additionally, Dz produced an equivalent increase in FP oxidation in control myocytes (Figure 3D) as compared to a blunted FP

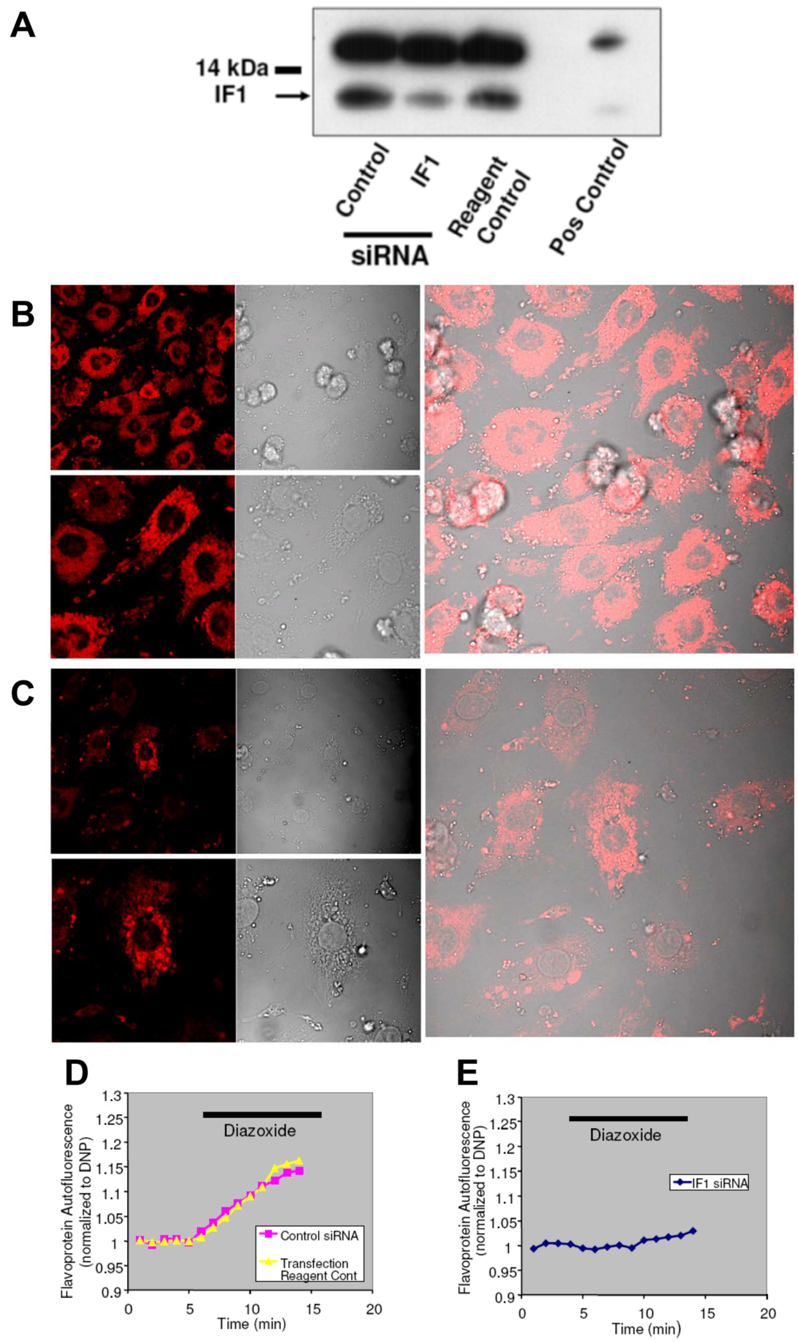

Figure 3. Knockdown of IF_1 expression in neonatal cardiomyocytes using RNA interference. (**A**) Western blot analysis of control vs siRNA treated samples; positive control corresponds to adult rat heart. (**B**) IF_1 immunocytochemical labeling of control, and (**C**) IF_1 siRNA treated cells. FP autofluorescence (normalized to 2,4-dinitrophenol, DNP) as marker of mK_{ATP} activity (**D-E**). (**D**) Dz induced flavoproteins oxidation in control, and (**E**) No effect of DZ was observed in IF_1 siRNA treated cells.

response from IF_1 siRNA treated cells (Figure 3E), consistent with F_1F_o functioning as a mK_{ATP} regulated by IF_1.

Mitochondrial K^+ flux and regulation of swelling and respiration

Since we have shown that F_1F_o naturally conducts K^+ in addition to H^+ ($P_K/P_H \sim 10^{-6}$), and that the normal cytoplasmic abundance of K^+:H^+ is $\sim 10^6$:1, we examined whether this mechanism could potentially serve a physiological homeostatic role in regulating mitochondrial K^+ influx, matrix

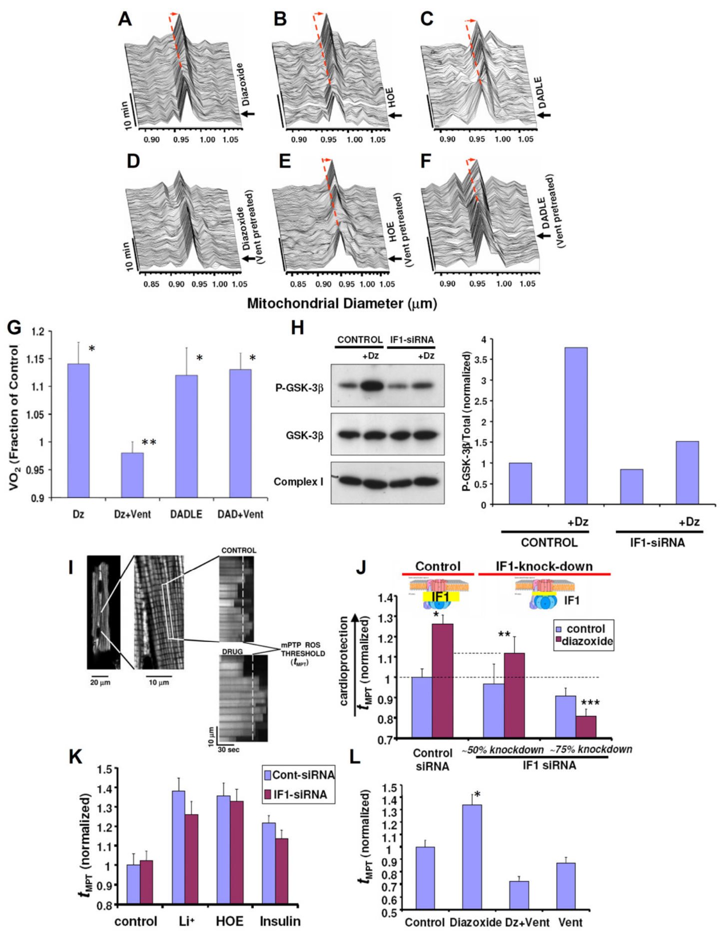

Figure 4. *In situ* monitoring of the amplitude and kinetics of regulatory mitochondrial swelling (resulting from increased mitochondrial K^+ influx and/or retention) in intact cardiomyocytes, based on Fourier analysis of laser linescan transmittance imaging. (**A**) KCO, Dz; see also Figure 4-figure supplement 1 and 2 regarding relationship between K^+ fluxes and mitochondrial volume changes. (**B**) The NHE-1 inhibitor, HOE, and (**C**) the δ-opioid peptide, DADLE, induced mitochondrial swelling. (**D**) The F_o inhibitor, Vent, blocked Dz-induced mitochondrial swelling, while it had no effect on swelling induced by (**E**) HOE or (**F**) DADLE. Arrow indicates the time point of drug addition. (**G**) Mitochondrial respiration (indexed by oxygen consumption, VO_2 with respect to Dz and Vent treatment as in **D**) in myocytes. (**H**) mK_{ATP} (Dz)-protection signaling via GSK-3β requires IF_1 (see text for details). While the KCO, Dz, causes a robust increase in P-GSK-3β in control cells, this was largely prevented in IF_1-siRNA treated cells. (**I**) Measurements of the mitochondrial permeability transition ROS threshold (t_{MPT}, the index of cardioprotection) in myocytes (used in **J-L**); typical positive t_{MPT} effect of a protective drug is illustrated vs Control. (**J**) t_{MPT} decreases in proportion to the degree of IF_1 knock-down, compared to control cells. (**K**) GSK-3β-dependent protection signaling which does not require mK_{ATP} activated K^+ flux (i.e., Li^+, HOE, insulin) is unaffected by IF_1-knock-down. (**L**) Block of F_o by venturicidin (Vent) prevents mK_{ATP} (Dz)-mediated cardioprotection. * $P<0.05$ vs paired Control; **,*** P=ns vs paired control.

volume and energy supply. Simultaneous monitoring of K^+ fluxes, volume and $\Delta\Psi_m$ was performed in isolated, respiring heart mitochondria (energized with glutamate/malate in KCl-based isotonic medium) in response to the classical state 4 → state 3 transition of respiration. Under these conditions, inhibiting F_1F_o with oligomycin reduced the total K^+ influx by at least 60%, and the consequent loss of osmotic drive allowed a 3-fold higher matrix contraction compared to matched controls (Figure 4 - figure supplement 1 and 2). Together with the calculation of the K^+ to H^+ conducted by F_1F_o (see Results section, "Measurements of unitary K^+ and H^+ currents from F_1F_o"), these data demonstrate the important new finding that K^+ transport carried by F_1F_o shares a significant portion of the K^+-osmotic cycle associated with the control of mitochondrial matrix volume while contributing to ATP synthesis during the transition from low to high energy demand states.

KCO-driven activation of mK_{ATP} causes mitochondrial swelling (Garlid et al, 2003) which in turn increases respiration (Halestrap, 1989; Korge et al, 2005). Using a novel single cardiac myocyte imaging technique (Juhaszova et al, 2004), we have found that KCO Dz, HOE694 (HOE; NHE-1 inhibitor), and the δ-opioid peptide, DADLE, each cause a rapid ~2.5-4% increase in the average volume of mitochondria throughout the cardiomyocyte and increase in respiration (Figure 4A-C;G). In cardiac myocyte suspension, we found that pharmacologic agents that cause mitochondrial swelling (Dz, HOE, and DADLE) increased oxygen consumption (VO_2) over baseline by about 10%, 25-30%, and 35%, respectively, when utilizing glucose, the medium- and long-chain fatty acid octanoate or palmitate, respectively, and that by preventing this volume increase (e.g., using the Cl^- channel inhibitor, IAA-94) the accompanying increase in respiration was similarly eliminated (Juhaszova et al, 2004). Thus, volume activation of respiration is a direct correlate of mitochondrial regulatory volume swelling. Using the same logic as the preceding section, since DADLE causes similar and rapid increases in respiration (as Dz) but is known to *not* activate the mK_{ATP}, it was employed as a negative control in the next series of experiments. We found that Vent completely prevented the Dz-related increase in cardiomyocyte swelling and respiration (Figures 4D,G), while the actions of HOE or DADLE were unaffected (Figures 4E-G). Thus, only the specific effect of Dz acting through the mK_{ATP} to cause mitochondrial swelling leading to an increase in respiration, but not that of DADLE, requires the function of F_o.

Effects on mPTP ROS-threshold

The mPTP is a key end-effector of protection signaling: the threshold for mPTP-induction by ROS being significantly reduced after ischemia-reperfusion injury and contributing to cell death, but beneficially increased by preconditioning, postconditioning and other forms of protection signaling, contributing to cell survival (Juhaszova et al, 2004; Juhaszova et al, 2009). We showed that cell protection involves convergence of a multiplicity of potential and distinct upstream pathways (including opening of mK_{ATP}), each acting via inhibition of GSK-3β on the end effector, the mPTP complex, to limit its induction (see Figure 4H-K). The activity of GSK-3β is inversely related to the phosphorylation status of serine (Ser)-9. Dephosphorylation of this site, or mutations that prevent phosphorylation, result in activation of the kinase (Antos et al, 2002). We found that constitutive activation of GSK-3β prevents the ability to engage protective signaling in cardiomyocytes through pathways including PKA, PKB, PKC, PKG and p70s6K. We also found that Dz (as well as numerous other distinct protection-signaling triggers (Juhaszova et al, 2004)), resulted in GSK-3β phosphorylation on regulatory serine-9 (including the fraction isolated from mitochondrial membranes). Thus, in the present experiments we compared the ability of Dz to phosphorylate GSK-3β on regulatory Ser-9 in cardiomyocytes with IF_1-expression knocked down by ~75% through siRNA, compared to controls. While Dz causes a significant increase in P-GSK-3β in control cells, this was largely prevented in IF_1-siRNA treated cells (Figure 4H). We conclude that mK_{ATP}-related protection signaling via GSK-3β requires the functional presence of IF_1, thus implicating the role of the F_1F_o. Further support for this role comes from the ability of Vent to similarly block phosphorylation of GSK-3β by Dz.

We have found that Dz, HOE, Li^+ (a direct pharmacologic inhibitor of GSK-3β), and insulin, each cause a significant increase of the ROS-threshold for mPTP induction, $\mathbf{t_{MPT}}$ (Juhaszova et al, 2004) (Figures 4I-L). Since HOE, Li^+ and insulin each cause protection via mK_{ATP}-independent mechanisms they were employed as negative controls in the next series of experiments. The degree of protection (i.e., prolonged $\mathbf{t_{MPT}}$) afforded by HOE, Li^+, and insulin was largely unaffected by IF_1-knockdown (Figure 4H,J,K). In stark contrast, the effect of Dz was decreased in direct relation to the degree of IF_1-knockdown, i.e., $\mathbf{t_{MPT}}$-increase was reduced by about half with ~50% IF_1-knockdown, and completely abolished with ~75% IF_1-knockdown (Figure 4H,J). We conclude that mK_{ATP}-related protection signaling to the mPTP requires the functional presence of IF_1, thus implicating the role of ATP synthase. This is compatible with a recently demonstrated role of IF_1 in cytoprotection (Campanella et al, 2008; Formentini et al, 2012). Furthermore, similarly to IF1-knockdown, Vent blocked the protection by Dz (Figure 4L). However, while blockage of F_o by Vent prevents mK_{ATP} (Dz)-mediated cardioprotection, it does not do so in the case of DADLE or HOE.

Regulation of F_1F_o by Bcl-xL and Mcl-1

Suspecting that the effect of Dz and pinacidil via IF_1 could be naturally operating under the control of yet-to-be discovered endogenous ligands of IF_1 we set out to find them. We examined IF_1 for conserved survival protein-related homology domains since IF_1 is known to have a "minimal inhibitory domain" sequence of 33 amino acids that binds to the β-subunit of F_1 (Gledhill et al, 2007). We found that IF_1 contains a conserved BH3-like domain (residues 32-46) that significantly overlaps its minimal inhibitory sequence (residues 14-47) (Figure 5A), and that Bcl-xL (Figure 5B,D) and Mcl-1 (Figure 5D), which are each known to have a BH3-binding groove, exert effects comparable to Dz on the H^+ and K^+ ion currents sustained by ATP synthase (Figures 5B-D). Furthermore, the effect of Bcl-xL and remarkably also of Dz, are reversed by a 26 AA peptide consisting of the BH3-domain of Bad (BH3 peptide, known to have nM affinity for Bcl-xL, but 1-2 orders less so for Bcl-2 (Kelekar et al, 1997; Petros et al, 2001)). A single AA substitution in the BH3 peptide (L12A), that reduces the affinity for Bcl-xL by almost 2 orders of magnitude (Wang et al, 2000), eliminated the inhibitory effects (Figure 5C). Notably, unlike Bcl-xL, Bcl-2 has no effect on F_1F_o H^+ and K^+ ion currents, which agrees with their known affinities for the BH3-domain of Bad, respectively. In binding experiments measuring changes in intrinsic tryptophan fluorescence, we found that Bcl-xL has a high affinity (sub-nM K_d) for the ligand IF_1, whereas Bcl-2's affinity is several orders of magnitude lower (see Material and methods, section Protein binding (Kd) measurements). These data suggest that IF_1 harbors a functionally-active BH3 domain homologous to that of Bad that overlaps with part of IF_1's inhibitory domain and functions as the area of binding to the β-subunit of F_1. Additionally, Bcl-xL and Mcl-1, but not Bcl-2, serve as endogenous regulatory ligands of ATP synthase via interaction with IF_1 at the BH3-like domain.

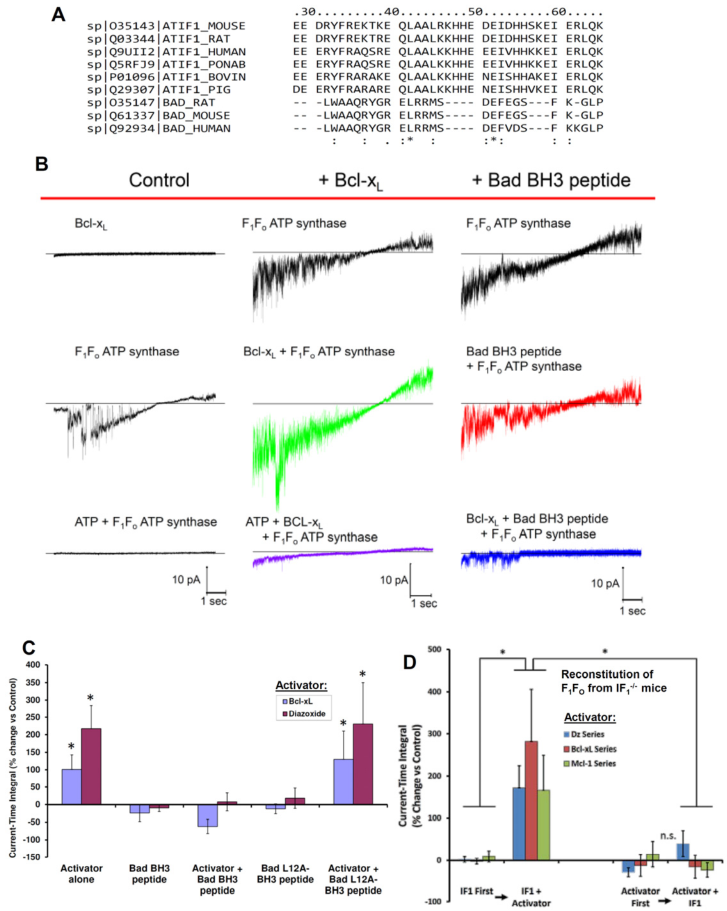

Figure 5. Regulation of F_1F_o activity by Dz, Bcl-2 family peptides and proteins mediated by IF_1. (**A**) AA alignment of the 26 residue BAD BH3 peptide and F_1F_o inhibitory factor IF_1 from mouse, rat, bovine, pig, monkey and human. The consistency of the alignment is indicated in the last row (asterisk shows complete conservation) (see also Supplementary file 2-figure supplement 1). BH3 peptide L12 aligns with L42 in full length IF1. (**B**) Effect of Bcl-xL (20 nM) and BH3 peptide (20 nM) on the voltage ramp (from -60 mv to +60 mV) evoked F_1F_o currents. Bcl-xl and BH3 peptide (middle and right traces, respectively; control current (left traces)). Bottom traces correspond to 2 mM ATP inhibited F_1F_o current. (**C**) Effect of Bcl-xL and Dz (30 µM) on the current-time integral of voltage ramp evoked F_1F_o currents. Control peptide with a single AA substitution L12A has no effect. (**D**) Effect of IF_1 reconstitution (100 nM), Dz, Bcl-xL and Mcl-1 on the current-time integral of voltage ramp evoked F_1F_o currents from $IF_1^{-/-}$ mice. The order of addition of IF_1 and Dz or Bcl-xL is varied among the various groups as indicated. * $P<0.05$ vs paired Control; **,*** P=ns vs paired control.

Regulation of ATP synthase by Bcl-xL, Mcl-1 and Dz requires IF_1

Thus far, we have discussed the role and function of IF_1 in intact cells, organelles and purified single molecules of F_1F_o, as well as in IF_1-knockdown experiments. Next, we examined the regulation of F_1F_o by Bcl-xL, Mcl-1 and Dz in the absence of IF_1, and upon reconstitution with IF_1. We measured H^+ and K^+ currents in F_1F_o isolated from $IF_1^{-/-}$ mice (see Figure 5D- figure supplement 1) regarding the $IF_1^{-/-}$ mice generation and confirmatory proof of lack of IF_1 expression) and the baseline properties of the ionic currents were essentially similar to that of WT control. Importantly, upon reconstitution with IF_1, P_H and P_K as well as total current reversal potential were found to be unchanged. One notable difference, however, was the ability of graded mM ATP amounts (by the energy transferred via its hydrolysis) to produce sufficient mechanical counter-torque (exerted by F_1 on the γ shaft) in excess of the oppositely-directed electrogenic mechanical torque exerted by F_o, causing a net reversal of electrical current in the $IF_1^{-/-}$ case (resulting in ATP hydrolysis-generated reverse ion pumping). The latter (i.e., ATP-generated reverse ion pumping) was not observed in parallel experiments with WT and is entirely consistent with the known function of IF_1 to limit the waste of futile ATP hydrolysis by impaired mitochondria under circumstances when $\Delta\Psi_m$ would drop below levels needed to synthesize ATP (Walker, 1994).

Assessing the current-time integral function (CTI, which in the direction of negative current is the direct analog of the amount of ATP synthesized) after reconstitution of F_1F_o with IF_1 in $IF_1^{-/-}$, we observed a small *increase* of ~11-14% in CTI (*vs* baseline). Thus, it is notable that IF_1 does not cause a *net* inhibitory drag on the energy transfer in F_1F_o likely due to frictional losses in the direction of ATP synthesis (see also discussion below regarding BH3 peptide effects). In contrast to WT, neither Dz, Bcl-xL nor Mcl-1 exerted a significant positive augmentation of CTI in the absence of IF_1, and subsequent IF_1 reconstitution was similarly ineffective (Figure 5D). A likely explanation for the apparent ineffectiveness of IF_1 added after Bcl-xL, Mcl-1 or Dz can be given by the possible interference exerted by these molecules on the intrinsic disorder of IF_1 (Bason et al, 2014), hindering its interaction at the F_1's binding cleft and γ shaft into a functionally active complex. In one case, the 5-fold excess of IF_1 used leaves effectively no free Bcl-xL because of the high affinity of this pair, and presumably only free IF_1, rather than bound, is able to reconstitute F_1F_o. In the case of Dz, this molecule could directly affect the intrinsic disorder of IF_1 or the binding cleft preventing effective reconstitution. On the other hand, prior reconstitution of F_1F_o with IF_1 restores the WT behavior entirely, with Dz, Bcl-xL and Mcl-1 manifesting a robust augmentation of CTI. Taken together, these data allow us to conclude that IF_1 is required for these mediators to augment F_1F_o activity (for the same driving force).

As stated earlier, the positive effects of Bcl-xL and Mcl-1 on WT F_1F_o currents could be reversed by the BH3 peptide (but not by the L12A variant, null-acting control BH3 peptide). Since this BH3 peptide, as well as IF_1, likely binds to the same region of F_1-β, but because of its short length is unable to reach to the γ shaft, we examined the functional effects upon binding F_1F_o in the absence of IF_1. We found that in IF_1-deficient F_1F_o, the BH3 peptide alone exerts a robust positive effect comparable to that of Dz, Bcl-xL and Mcl-1 (i.e., doubling to tripling the activity), but the L12A-modified BH3 peptide had no effect, suggesting that IF_1 likely produces significant frictional drag via its constitutive contact with the γ shaft that is fully offset by some function-augmenting mechanism achieved by the portion of IF_1 bound to F_1-β (see below and Discussion).

Regulation of mechano-chemical efficiency of F_1F_o

We have shown that F_1F_o, conducting univalent cations at a fixed driving energy, Δμ, can be upregulated to increase the total ion flux against a constant load without slip or leak via the IF_1-dependent actions of synthetic small molecules such as Dz and pinacidil, and endogenous proteins such as Bcl-xL and Mcl-1. The absence of slip is revealed by complete inhibition of currents at high Δμ by excess ATP. This activity enables ATP synthase to function as a recruitable mK_{ATP}, whereby the triggered increase of mitochondrial K^+ influx and matrix volume upregulate respiration and produce redox activation of local signaling inhibiting GSK-3β and resulting in desensitization of the mPTP to damaging levels of ROS (Juhaszova et al, 2004; Zorov et al, 2014). These data, together with the results showing that Bcl-xL and Dz (and pinacidil and Mcl-1) are

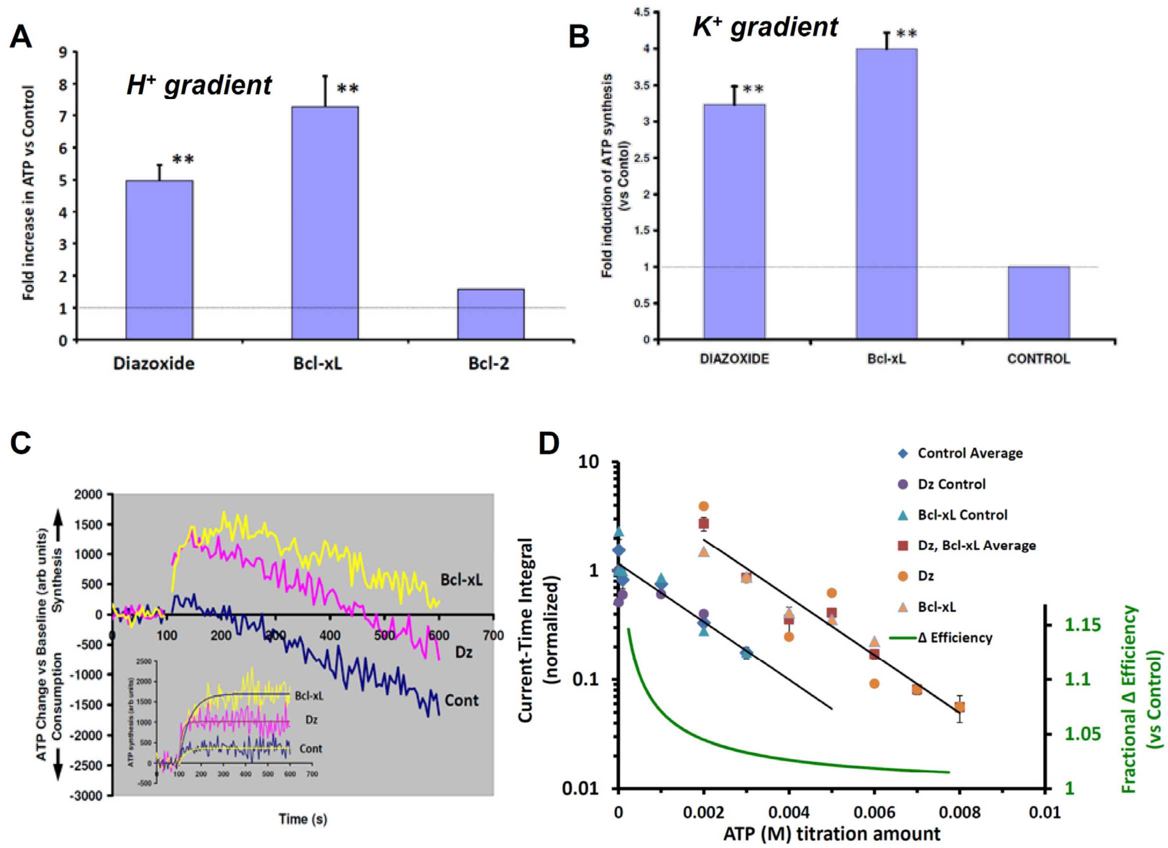

Figure 6. Regulation of mechano-chemical efficiency of F_1F_o. F_1F_o activity driven by a H^+ (**A**) or a K^+ gradient (**B**) in PL. (**C**) ATP production/consumption kinetics (chemiluminescence) in a K^+ gradient in PL. (**D**) Dose-response of ATP inhibition of F_1F_o (H^+) currents and Dz and Bcl-xL activated F_1F_o currents: *x-axis-(linear)* ATP concentration used for inhibition of F_1F_o currents, *y-axis (log)* normalized current-time integral of F_1F_o currents. Dz and Bcl-xL produced a parallel shift in the F_1F_o activity vs control resulting in the energy of an additional ~2.8 mM ATP being required to provide sufficient counter-torque to limit F_1F_o to the same level of function as under control conditions. The relative change in efficiency was calculated as the ratio of the free energy of ATP hydrolysis during activation by Dz and Bcl-xL over that under basal conditions. * P<0.05, ** P<0.02.

each capable of increasing the amount of ATP synthesized by reconstituted F_1F_o (WT, IF_1-competent) utilizing either K^+ or H^+ gradients (Figures 6A-C), suggest that these IF_1-dependent effectors have increased the mechano-chemical efficiency of the ATP synthase. To investigate this, we examined the titration curve of the CTI (at each of the ion-reversal potentials for H^+ and K^+, in single ATP synthase molecules) as a function of the counter-torque on the γ shaft applied by F_1 resulting from the hydrolysis energy derived from increasing ATP concentrations, in the presence of Dz or Bcl-xL as compared to controls. The data obtained are well described by a log-linear relationship between CTI and [ATP]. Dz and Bcl-xL produced a parallel upward shift of 5.6-fold in the F_1F_o activity *vs* control (Figure 6D) indicating that the hydrolysis energy of an additional ~2.8 mM ATP is required to provide sufficient counter-torque to constrain the F_1F_o to the same level of function as under control conditions. Based on considerations of energy conservation, the additional ATP synthesis might be driven by extra energy that was not lost to viscous drag and intermolecular friction. Together, these results are in agreement with the idea that both Bcl-xL and Dz increase the mechano-chemical efficiency of ATP synthase (e.g., by ~7% at 1 mM, ~5% at 2 mM, and ~3% at 4 mM ambient ATP).

Discussion

Up to the present, it has been a central tenet of bioenergetics that mammalian ATP synthase operates solely on proton flux through F_o to make ATP. The present work significantly revises that concept. We found that in spite of the high degree of F_o's H^+ selectivity vs K^+ (~10^6:1), the abundance of cytoplasmic K^+ over H^+ being >10^6:1 enables ATP synthase to harness $\Delta\mu_K$ (electrical gradient energy) and conduct a significant number of K^+ for every H^+ in the synthesis of ATP. This has major implications for thermodynamic efficiency of energy transduction. What we propose all remains fully compatible with Mitchell's chemiosmotic mechanism (Mitchell, 1961); reviewed in (Nicholls & Ferguson, 2013).

We demonstrated that purified F_1F_o is utilizing up to 3.7 K^+ for every H^+ transferred. As such, the ATP synthase acts as a K^+-uniporter, i.e., the primary way for K^+ to enter mitochondria; furthermore, since this K^+ entry is directly proportional to ATP synthesis and regulates matrix volume and respiration, in turn it serves the function of directing the matching of cellular energy utilization with its generation. Chemo-mechanical efficiency of ATP synthase can be up-regulated by certain members of the Bcl-2 family and by certain K^+ channel openers acting via an intrinsic regulatory factor of ATP synthase, IF_1, in a process that increases the monovalent cation conductance of F_1F_o while retaining its high degree H^+-selectivity. The K^+ flux can be enhanced, halted, or even reversed depending on ATP concentration based on thermodynamic energy balance. Because of this, we found that ATP synthase is also a recruitable mK_{ATP} which serves critical functions in cell protection signaling. It can limit the damage of ischemia-reperfusion injury via redox activation of local signaling to desensitize the mPTP to damaging levels of ROS. The fundamental importance of these findings cannot be overstated since ATP synthase constitutes the main energy transduction mechanism in most living systems, including humans where it makes the daily equivalent of approximately the body's weight in ATP.

We show that F_1F_o, conducting H^+ and K^+, can be upregulated (even at the same driving energy, $\Delta\mu$) to increase the total ion-flux (at constant H^+:K^+) against a constant load without slip or leak (Figure 7), via the IF_1-dependent actions of endogenous pro-survival proteins, Bcl-xL and Mcl-1, and Dz and pinacidil. Increasing ATP synthesis driven by K^+- and H^+-influx through F_o provides a way for F_1F_o to operate as a mitochondrial K^+-uniporter to regulate matrix osmotic balance while matching metabolic energy supply with demand. Directly coupling ATP synthase activity to quantitative K^+ matrix-influx and hence to the osmotic drive, regulation of matrix volume and, in turn, of the respiratory chain, affects a logically efficient energy supply-demand matching system. In particular, by harnessing $\Delta\mu_K$ converted from respiratory chain-generated $\Delta\mu_H$ through the activity of the KHE, F_1F_o generates additional ATP proportional to the amount of energy that would have been dissipated as heat by the same K^+ current in passing (in a hypothetical scenario) through a separate entity functioning only as a K^+ uniporter. In other words, letting K^+ enter via a non-ATP generating process would not be as energetically effective as using the F_1F_o as the K^+-influx mechanism. Thus, once the K^+ is eventually extruded by the KHE using H^+ influx, the equivalent energy of that H^+ will have been harnessed in form of ATP made by the K^+ influx through the F_1F_o (Figure 7B).

Our electrophysiological measurements indicate that purified F_1F_o reconstituted into the lipid bilayer could conduct up to 3.7 K^+ for every H^+, in the absence of any other K^+ conducting pathway

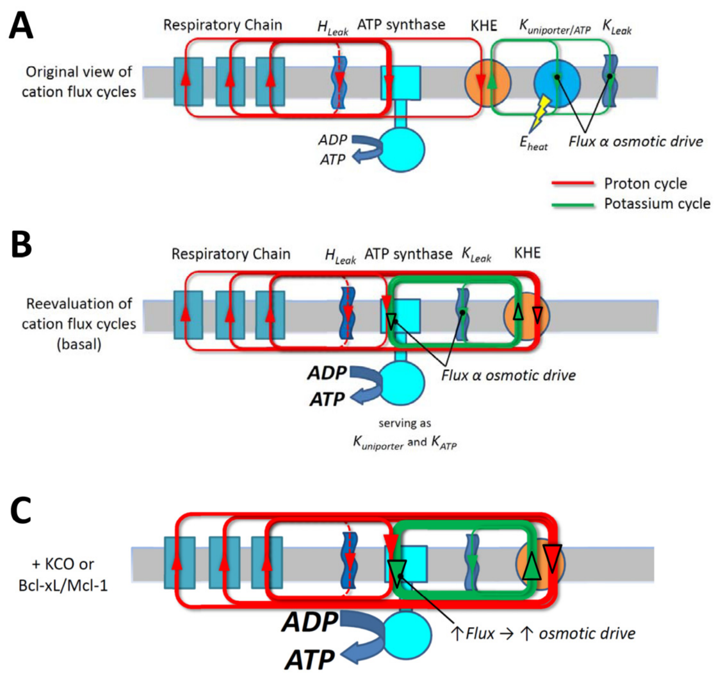

Figure 7. **Scheme of the H^+ and K^+ transport across the inner mitochondrial membrane.** From the energetic standpoint, all the energy available to perform work and execute the ionic movements derives from the original H^+ gradient established by proton pumps in the respiratory chain. A central point is the obligatory preservation of charge and mass balance under the steady state circuits. In the "original view of cation flux cycles" (**A**), a certain (majority) of the H^+ gradient is being harnessed by F_1F_o directly to make ATP, whereas a certain amount of K^+ is entering the matrix through an ordinary K^+ channel mechanism (a "mK_{ATP}-uniporter" channel), driven by $\Delta\Psi$, and extruded via KHE utilizing the energy remaining in the fraction of the H^+ gradient not harnessed by F_1F_o. The equivalent energy of this fraction being used to extrude K^+, and a large fraction of that non-ATP-producing energy would essentially be dissipated as heat in the constant cycle of K^+ recirculation (green circuit in **A**). In the new mechanism (**B**) the same amount of energy available in the original H^+ gradient but largely lost as heat is entirely available to produce ATP, simply by having the mK_{ATP}-uniporter mechanism reside inside, and as natural part of, F_1F_o with the traffic of H^+, K^+ or even Na^+ contributing its energy to producing ATP. The remainder of the H^+ gradient energy is now utilized to remove all the K^+ that entered via F_1F_o (n.b., this exchange process of extruding K^+, restoring $\Delta\mu_K$, is the way that the H^+ gradient energy is still the original, entire driving force for ATP production). However, the gain is that more ATP is produced for the same input energy by not wasting some of that energy on maintaining what was originally thought to be a separate K^+ cycle that does not/cannot generate any ATP. Engineered this way, it is a better, tightly coupled system of energy supply-demand matching through the K^+ cycle utilizing F_1F_o because the matrix influx of K^+ is truly directly proportional to ATP synthesis. Any transient increase in F_1F_o activity will thus lead to transient K^+ accumulation (due to a natural kinetic lag in the activity increase in KHE reacting to the matrix K^+ accumulation). This will lead to the attraction of a counter-ion and change of the osmotic drive yielding a "volume-activation of respiration" response which previously has been documented in detail (Juhaszova et al, 2004). The scheme depicted in (**C**) integrates the implications of modestly enhancing the chemo-mechanical efficiency of F_1F_o (by KCO's or Bcl-xL/Mcl-1). For the driving energy of the same H^+ gradient the F_1F_o flux increases, enabling increased respiration and a directly increased K^+ flux cycle (yielding an increased volume signal) and enhanced ATP generation (**C**) vs the basal conditions (**B**).

as demonstrated (Figure 6D). In isolated mitochondria no less than 60% of the K^+ flux is sustained by the ATP synthase (Figure 1-figure supplement 2A,B), thus showing that F_1F_o is a major mitochondrial K^+ influx pathway. Because a transient change in K^+ influx would need to be matched by influx of a counter-ion (e.g., Cl^-) to produce an osmotic imbalance signal, both KHE and the counter-ion transport pathways are also important control steps in matrix volume regulation. Dysfunction of mitochondrial KHE activity leads to aberrations in matrix K^+ and mitochondrial volume regulation that in turn may affect fission/fusion and mitophagy. Such pathology is evident in the Wolf-Hirschhorn syndrome, a genetic insufficiency of mito-KHE activity (1/50,000 incidence, characterized by microcephaly, growth retardation, intellectual disability, and epileptic seizures among other severe manifestations (Zotova et al, 2010)).

The K^+ uniporter function also enables F_1F_o to operate as an on-demand, recruitable mK_{ATP}, whereby triggered increases of mitochondrial K^+-influx and matrix-volume upregulate the signaling cascade resulting in desensitization of the mPTP, enhancing cell survival (Juhaszova et al, 2004). Nature usually operates important pathways with built-in redundancy so that other mitochondrial K^+ channels may contribute to these mechanisms, including the Ca^{2+}-activated K^+ channel, BK_{Ca} (Xu et al, 2002), and a ROMK channel which may also mimic mK_{ATP} channel function (Foster et al, 2012), but these pathways are likely fine-tuning mechanisms.

Our data also unveil that F_1F_o operates at increased efficiency (by up to ~7% at normal ATP levels) in response to KCOs, Bcl-xL and Mcl-1, yielding both increased ATP output and matrix K^+ influx for the same $\Delta\mu_H$ (Figures 6A-C; Figure 7C). Dz and Bcl-xL cause a rightward shift in the ATP-dependence of the CTI (a quantitative index of ATP synthesis), such that the hydrolysis energy of an additional ~2.8 mM ATP is required to provide sufficient counter-torque to constrain the F_1F_o to the same level of function as in controls. This means that an additional ~2.8 mM ATP can be produced for the same input energy at normal ambient levels of ATP. This provides quantitative proof that both Bcl-xL and Dz increase the mechano-chemical efficiency of F_1F_o (Figure 6D). Recent work found that Bcl-xL interacts with the F_1F_o (Alavian et al, 2011; Formentini et al, 2014), specifically with the β-subunit of ATP synthase decreasing an ion leak within the F_1F_o complex and concluded that this was responsible for increasing net transport of H^+ by F_1F_o (Alavian et al, 2011). These latter findings and conclusions are non-trivially different from our experiments: (1) we do not observe ion leak (or slip) at all, regulated or otherwise, in F_1F_o in the presence or absence of Bcl-xL, i.e., Bcl-xL does not inhibit an ion leak that is not present in ATP synthase, and (2) the increase in ATP synthetic capacity in response to Bcl-xL is specifically due to an increase in mechano-chemical efficiency of ATP synthase *per se*, and not by changing an ion leak into useful energy. These findings lead us to conclude that essential mitochondrial homeostatic and pro-survival mechanisms result from a regulated IF_1-mediated increase in chemo-mechanical efficiency of F_1F_o conducting both K^+ and H^+. Our results add a significant dimension to the known, and apparently diverse biological function sets of F_1F_o. Additionally, it was proposed that a certain triggered rearrangement of F_1F_o dimers is functionally responsible for other major biological functions such as the mitochondrial cristae arrangements (Strauss et al, 2008) and the formation of the mPTP (Giorgio et al, 2013).

Our findings raise the question of how IF_1 might control the activity of ATP synthase to engage physiologic/homeostatic and survival-promoting mechanisms. Overall, our data are consistent with a "minimal inhibitory domain" of IF_1 (residues 14-47 in bovine IF_1 (van Raaij et al, 1996)) binding to the β-subunit of F_1 in an "IF_1 ligand-binding cleft" (adjacent to the F_1 α-subunit interface), forming at its proximal end an α-helix loop that interacts with the F_1 γ-rotor shaft which is responsible for limiting ATPase activity. With the evidence of a significant modulatory role by certain Bcl-2 members, we examined this domain for conserved survival protein-related homology domains. Bcl-xL and Mcl-1 are each known to have a BH3-binding groove with high affinity for certain domains of BH3. Together with the result of the high affinity binding of IF_1 to Bcl-xL, our data is in agreement with IF_1 harboring a functionally-active BH3-like domain homologous to that

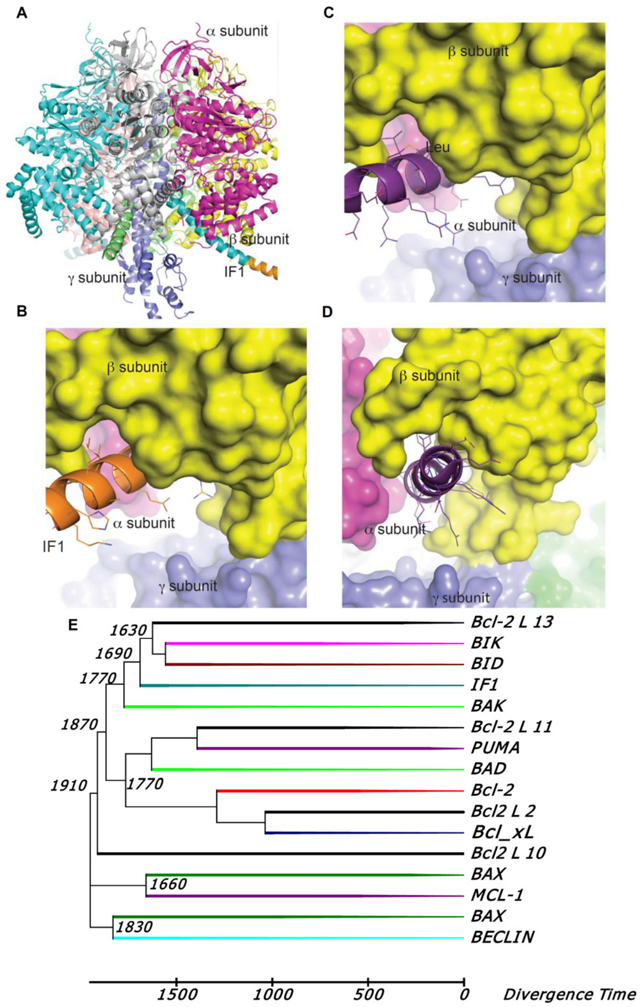

Figure 8. **Interaction of F_1 ATPase with IF_1 or a BH3 modeled peptide.** (**A**) Ribbon model of the crystal structure of bovine F1 (PDB ID 4Z1M) emphasizing two of the three β subunits (cyan and magenta) and the γ subunit (blue) in interaction with the long α-helix of the inhibitor protein IF_1 (orange). The IF_1 domain (residues 18-51 are shown in cyan; residues 23-70 from PDB ID 1GMJ are shown in orange) interacts with the β subunit marked in yellow. (**B**) Surface representation of subunits β (yellow) and α (magenta) of F_1 ATPase interacting with IF_1 peptide. (**C**) As panel **B** with the peptide α_2 from the BAD protein (PDB ID 1G5J, as it binds BCL-XL) in ribbon representation at the IF_1 groove in F_1 showing the aliphatic side chain of Leu 42 in IF_1 and Leu 12 in BH3-BAD peptide (corresponding to Leu 114 in human BAD). (**D**) Same as **C** at an approximately 90° orientation. (**E**) Phylogenetic tree of the BH3 extended peptides (35 residues) from Bcl-2 proteins and IF1 across eukaryotes. Sequence alignment was computed with Clustal Omega (Sievers et al, 2011) and the tree and divergence times (in Myr) were calculated by MEGA 6.0 (for further details see Figure 8-figure supplements 1-3, and Table 1).

of Bad and coincident with IF_1's inhibitory domain that functions as the binding patch to the β-subunit of F_1. Binding of Bcl-xL and Mcl-1, but not Bcl-2, via IF_1 interaction, endogenously regulate F_1F_o activity. This may explain why the effects of Bcl-xL, Mcl-1, and Dz, are reversed by the BH3 peptide, but not by the same peptide with a single AA change (L12A) (Kelekar et al, 1997; Wang et al, 2000) (Figure 5C). Specifically, the BH3 peptide may compete and displace IF_1 from its binding site on F_1F_o, as well as interfere with its binding to Bcl-xL or Mcl-1. Moreover, we have shown that, unlike in WT, neither Dz nor Bcl-xL significantly increased CTI in F_1F_o from

$IF_1^{-/-}$. Alternatively, prior reconstitution of F_1F_o in the presence of IF_1 entirely rescued the WT behavior, with both Dz and Bcl-xL strongly augmenting the ion currents. These data allow us to conclude that the higher ATP synthase activity elicited by these effectors (for the same driving force) requires IF_1, and that the mere removal from its binding site does not suffice to enhance the enzyme activity. We propose that in the normal basal state IF_1 has two mechanical and *nearly offsetting* effects on the function of ATP synthase operating in the synthesis direction: (1) a net *negative*, frictional drag-like effect of the IF_1 molecule originating at its proximal end where it engages the γ shaft in its natural rotation, and (2) a net *positive* effect created somehow by the presence of the long α-helical stretch that engages the IF_1 binding cleft on F_1-β, the latter effect being mimicked by the BH3-peptide. It has been shown that Bcl-xL can interact forming 3D-domain swapped (3DDS) homodimers (O'Neill et al, 2006) as well as heterodimers with other survival-regulating proteins. These interactions can significantly affect the residual function of both partners (Rajan et al, 2015), and certain BH3-only proteins can bind to and partially unfold Bcl-xL, changing its interactions with other binding partners and thereby biasing cell survival-signaling (Follis et al, 2013). Thus, our two-fold proposal implies that (1) Bcl-xL/Mcl-1 (via their intrinsic BH3-binding grooves) tightly bind to IF_1 at its minimal inhibitory/BH3-like domain to displace it from its binding cleft at F_1-β, and (2) this interaction triggers a specific unfolding and rearrangement of the Bcl protein's α_2 helix, enabling an increase of its potential range-of-motion. This could allow the helix from the Bcl protein to participate in an energetically favorable rearrangement with F_1F_o by binding to the empty IF_1 binding cleft. We propose a possible model of this interaction (Bcl-protein's α_2 helix containing its BH3 domain engaging the IF_1 binding cleft on F_1-β; Figure 8) that would cause the Bcl-xL/Mcl-1-mediated increase of F_1F_o function in the presence of IF_1, analogous to that obtained with the BH3 peptide added to the IF_1 deficient F_1F_o (Figure 5D). The mechanism by which a short IF_1/BH3-(like) helical-peptide structure occupying the natural IF_1 binding groove can enhance the chemo-mechanical efficiency of F_1F_o is of considerable interest, but how it specifically works remains a matter of future study.

The origin of IF_1 in relation to the evolution of F_1F_o is also an interesting question. There are conserved "IF_1 domains" that can be found embedded in a variety of larger proteins across Archaea, Bacteria, and Eukaryotes (Geer et al, 2002), suggesting ancient origins for this domain. Although F_1F_o exists in all major lifeforms, IF_1 as a separate entity is only known to regulate synthase function in Eukaryotes. It is tempting to speculate that when the early bacterium became a mitochondrion as a functional organelle of the eukaryotic cell, some 2 billion years ago, it brought along the genetic information for IF_1, which might have evolved to prevent the mitochondrion from wasteful ATP consumption in the host cell. We examined these bacterial IF_1-progenitors and they have regions homologous to the BH3-like domains that we found in eukaryotic IF_1's. The Bcl family is also ancient, some 2 billion years extant and resident in eukaryotic lifeforms. Phylogenetic analysis shows that IF_1 is actually an ancient member of the Bcl family and today may be most closely related to BH3-containing proteins (e.g., Bad, PUMA, Bcl-xL; Figure 8E; Figure 8-figure supplements 1-3, Table 1). This may explain how the Bcl-2 protein family has come to regulate F_1F_o function as part of its repertoire of survival-regulating functions.

In conclusion, we demonstrated that F_1F_o utilizes the ion gradient energy not only of H^+ but also of K^+ to drive ATP synthesis. The essential mitochondrial homeostatic and pro-survival mechanisms discussed here, including F_1F_o operation as a primary mitochondrial K^+ uniporter to facilitate energy supply-demand matching, and as a recruitable mK_{ATP} channel to protect from pathological opening of the mPTP, result from regulated function of ATP synthase conducting both K^+ and H^+. The specific mechanisms by which KCOs and certain Bcl-2 family proteins engage IF_1 to produce an increase in the chemo-mechanical efficiency of ATP synthase will require additional investigation.

Material and methods

Cell isolation.
Adult cardiac myocytes were isolated from Sprague-Dawley rats (2–4 months old), and WT or IF_1 KO mice by using standard enzymatic techniques, as described previously (Capogrossi et al, 1986). Isolated cardiomyocytes were suspended in a solution containing (in mM): NaCl 137, KCl 4.9, $MgSO_4$ 1.2, NaH_2PO_4 1.2, glucose 15, HEPES 20, and $CaCl_2$ 1.0 (pH 7.4). Handling of animals was conducted in accordance with NIH guidelines for animal care and use.

Immunocapture isolation/purification of intact F_1F_o from rat heart mitochondria, and the functional reconstitution into proteoliposomes (PL).
All chemicals where from Sigma-Aldrich (St. Louis, MO), except where otherwise noted. Rat heart mitochondria were solubilized in 1% lauryl maltoside (LM; Anatrace Inc., Maumee, OH) or 1.5% - 2% digitonin for 10 min, unsolubilized material was removed by centrifugation at 25000 x g for 15 min. F_1F_o was immunocaptured using a Complex V immunocapture kit (MitoSciences Inc., Eugene, OR). Integrity and purity of the isolated F_1F_o was determined by gel electrophoresis under native and denaturing conditions. NativePage Novex 3-12% Bis-Tris gel system (Invitrogen Corp., Carlsbad, CA) was applied to analyze samples under native clear and native blue (0.002% Coomassie Blue G-250) conditions. Gels were silver or Coomassie stained, or blotted to a PVDF membrane (GE Healthcare Bio-Sciences, Marlborough, MA) for protein immunodetection.
Purified F_1F_o was reconstituted into proteoliposomes using a modified procedure based on a method developed originally by (Paucek et al, 1992). Briefly, for ATP measurements, cardiolipin and phosphatidylcholine in a 1:9 ratio were dried under nitrogen and dispersed at 100 mg/ml in an outwardly-directed potassium gradient was employed with an internal buffer containing (in mM): 10 NaH_2PO_4, 200 K_2SO_4 (or KCl; and Na_2SO_4 or NaCl), 0.25 EDTA, 20 HEPES, pH 7.0. Lipids were solubilized by octylpentaoxyethylene detergent. ~ 5 µg of isolated F_1F_o was added to 10 mg of solubilized lipids. Proteoliposome (PL) formation was induced by removal of the detergent in Bio-beads SM2 column (Bio-Rad Laboratories, Hercules, CA).

Rat mitochondria and submitochondrial membrane particles isolation
Mitochondria were isolated by differential centrifugation of the heart homogenate.
Fresh submitochondrial membrane particles (SMP) were made by sonicating rat heart mitochondria until cloudy preparation turns clear, then centrifugation at 16,000 x g for 15 minutes and subsequent centrifugation of the supernatant at 140,000 x g for 20 minutes to pellet the SMPs, which were resuspended in isolation medium. For electrophysiological measurements the isolated SMPs were added directly into the *trans* chamber.

Protein detection
BCA (bicinchoninic acid) protein assay (Pierce Biotechnology, Inc., Rockford, IL) was used for measurements of protein concentration.

Immunoblotting

For analysis under denaturing conditions, mitochondria or cells were lysed for 30 min on ice with RIPA buffer (0.15 mol/L NaCl, 10 mmol/L Tris (pH 7.4), 1 % NP-40, 0.1 % SDS, 0.5 % deoxycholate,1 mmol/L NaF, 1 mmol/L sodium orthovanadate) and protease inhibitors (Roche Diagnostics), and the lysates were centrifuged (25 min at 4°C; 25,000 x g). Lysates or purified F_1F_o were heated (10 min at 75 ºC) in the NuPage LDS sample buffer under reducing conditions. Proteins extracts were separated using pre-cast NuPAGE Bis-Tris 4-12% gels (Invitrogen). Gels were then silver stained or the proteins were transferred to a PVDF membrane. The membranes were blocked with 5% nonfat dry milk in tris(hydroxymethyl)aminomethane (Tris)-buffered saline with 0.1% Tween 20 (TBST) and incubated overnight with primary antibodies; followed by horseradish peroxidase-linked secondary antibodies (Amersham Biosciences, Piscataway, NJ). Protein bands were visualized using ECL system (Amersham Biosciences) diluted in TBST.

Antibodies used: P-GSK-3β (Cell Signaling Technology, Danvers, MA); GSK-3β, ANT (Santa Cruz Biotechnology, Dallas, TX) Complex I, Complex V subunits, IF_1 (AbCam, Cambridge, MA), KCNJ1 Sigma Prestige (Sigma-Aldrich).

Immunofluorescence

Cultured neonatal cardiac myocytes were fixed with 2% formaldehyde in PBS (phosphate buffered saline; Sigma-Aldrich) followed by permeabilization with 0.5% Triton X-100/PBS. We blocked nonspecific cross reactivity by incubating the samples for 4 h in 1% BSA/PBS (Jackson ImmunoResearch, West Grove, PA, USA) and then performed cell immunolabeling via incubation with primary anti-IF_1 antibody diluted in 1% BSA/PBS overnight, washing in PBS followed by appropriate fluorescence label-conjugated secondary antibodies (Jackson ImmunoResearch). Labeled cells were imaged by a Zeiss LSM-510 (Carl Zeiss, Jena, Germany) confocal microscope using a 63x/1.4 N.A. oil immersion lens.

ATP measurements

External buffer (EB) contained (in mM): 10 NaH_2PO_4, 200 TEA-SO_4 (or TEA-Cl), 2.5 $MgCl_2$, 0.090 ADP (ultra-pure; Cell Technology Inc., Mountain View, CA), 1 EDTA, 0.001 FCCP, 20 TEA-HEPES pH 7.0, and using a Vapro osmometer (Wescor, Inc., Logan, UT) the osmotic activity of the internal solution (K^+=200 mEq) was matched to that of the EB (K^+=0, TEA^+=200 mEq) with an appropriate amount of mannitol. 5 µl of formed PL was resuspended in 495 µl of EB. After 5 min incubation at room temperature the ATP production was determined by luciferase/luciferin system using ATP bioluminescence assay kit HS II (Roche Diagnostics GmbH, Penzberg, Germany) in a Tropix TR 717 microplate luminometer (Bedford, MA).

To measure ATP production/consumption kinetics we developed a novel on-command acceleration-triggered inertial injector system, contained entirely inside individual wells of a 96 well plate, capable of accurately and reproducibly introducing and admixing 1-2 µL volumes in 1-5 sec (as desired, and without optical interference) during continuous chemiluminescence recording protocols. Specifically, individual wells of a 96 well plate were loaded with 198 µL of EB (see above) supplemented with 30 µM luciferin (Sigma-Aldrich) and 30 pmol/well of luciferase (Promega Corp., Madison, WI); a meniscus-stabilized microcarrier containing 1-2 µL of PL (loaded with internal 200 K^+ buffer) was carefully placed on top of the EB. After the background-level luminescence was acquired (Victor3 plate reader; PerkinElmer Inc.; Waltham, MA), the ATP generating system (PL) was injected into the buffer-containing well (which initiates the ATP synthesis reaction). This method enables measurement the relatively fast reaction kinetics of ATP synthesis (from microliter reaction quantities) from baseline to completion of the reaction.

K^+ flux measurements

A similar procedure as described above was used to prepare PLs for determination of K^+ fluxes; additionally, vesicles were loaded with the potassium sensitive probe PBFI (Invitrogen). Extra-vesicular PBFI was removed by passing the vesicles through 2 ml Bio-Spin columns (Bio-Rad Laboratories, Hercules, CA), which had been pre-equilibrated with internal buffer without the probe. In these experiments, an inwardly-directed potassium gradient was employed and the internal buffer contained (in mM): 125 TEA-SO_4, 1 EDTA, 25 TEA-HEPES pH 7.0, and 0.3 PBFI. The osmotic activity of the internal solution (K^+=0) was matched to that of the external buffer (K^+=150 mEq) with an appropriate amount of mannitol, using an osmometer. 5 µl of suspension was transferred with vigorous stirring into a cuvette containing 495 µl: in mM 150 KCl, 1 EDTA, 25 HEPES, 1 µM FCCP, pH 7.0. PBFI-fluorescence ratio was measured continuously in a Perkin-Elmer LS 50B fluorescence spectrophotometer and the normalized initial rate of rise of the signal was taken as the index of K^+ influx.

In-gel ATPase assay

The in-gel ATPase assay described in (Wittig et al, 2006) was slightly modified: Clear native (CN) and blue native (BN)-gels were preincubated for 2 hr in 270 mM glycine, 35 mM Tris, pH 8.4. In a parallel assay, ATPase was inhibited with 5 µg/ml oligomycin. Gels were incubated for 45 min in ATPase reaction medium (in mM): 270 glycine, 35 Tris, 8 ATP, 14 $MgSO_4$, 0.2% $PbNO_3$, pH 8.4. Gels were washed with water and precipitated white lead phosphate bands were transformed to dark brown lead sulfide bands by immersion of the gels in 5% ammonium sulfide followed by a water rinse. Gels were then fixed (40% methanol, 10 % acetic acid) and protein visualized using a colloidal blue staining kit (Invitrogen).

Protein binding (K_d) measurements

For dissociation constant (K_d) measurements of IF_1 to Bcl-2-family proteins (Bcl-2, Bcl-xL), 100 nM of Bcl-protein was admixed with 0-200 nM of IF_1. Binding was monitored via changes in intrinsic Trp fluorescence, excited at 295 nm and fluorescence detected at 350 nm. Measurements were performed using a PTI (Photon Technology, Inc.) fluorimeter. Extracted intensities were fitted to a generalized binding equation:

$$F = F_0 + A \cdot \frac{([I]+[B_t]+K_d) - \sqrt{([I]+[B_t]+K_d)^2 - 4[I][B_t]}}{2[B_t]}$$

where $[B_t]$ is the total Bcl-protein concentration, $[I]$ is the concentration of IF_1, F_0 and A are background fluorescence and a scaling factor, respectively.

Cell and proteoliposome treatment

The following compounds were applied (alone or in combination) to cells and PL during experimental measurements: 3 mM LiCl (Calbiochem Corp., San Diego, CA, USA); 2-4 µM F_o-inhibitor venturicidin B (VENT; A.G. Scientific, Inc., San Diego, CA). MgATP (at various concentrations as indicated); 10 nM Tyr-D-Ala-Gly-Phe-D-Leu (DADLE); 100 µM glibenclamide; 30 µM diazoxide (Dz); 50 µM pinacidil; 500 µM 5-hydroxydecanoate (5HD); 1

μM oligomycin, 0.4-0.6 mM DCCD, 1 μM valinomycin; 1 μM FCCP; 20-100 nM Bcl-2, Bcl-xl and Mcl-1 (Sigma-Aldrich); 2 μM Bcl-2 binding peptide (Bad BH3 peptide) and its negative control (Calbiochem).

Electrophysiological measurements of unitary K^+ and H^+ currents from F_1F_o

Electrophysiological characterization of reconstituted F_1F_o was performed using conventional bilayer lipid membrane techniques (Planar Lipid Bilayer workstations (Warner Instruments, LLC; Hamden, CT)). Briefly, "black" lipid membranes were formed across a 200 μm aperture that separated the *cis*- and *trans*-compartments of a custom designed and fabricated chamber. The lipid ratio of phosphatidylcholine (PC) : phosphatidylethanolamine (PE) : cardiolipin (CL) was 4.5:4.5:1 by mass. Proteoliposomes were added to the *trans* chamber (simulating the cytosolic side) which was held at virtual ground and contained a solution composed of (in mM): 150 KCl, 20 Tris-HCl, 1 EGTA, 0.5 ADP, 10 PO_4^{3-} (with 50 μM DTT, pH 7.2). Measurements were made after spontaneous vesicle fusion and protein incorporation into the lipid bilayer membrane had been achieved. Voltage was applied (Warner BC-535 Bilayer Clamp amplifier) to the *cis* chamber (simulating the mitochondrial matrix) with the same composition as the *trans* solution except having 50 mM KCl. Single channel currents were filtered by a low-pass 8-pole Bessel filter at a corner frequency of 2 kHz and digitized at a sampling rate of 50 kHz. All measurements were obtained at room temperature (22-23°C).

Measurements of the mitochondrial volume in intact cells

Transmitted optics line-scan imaging to assess changes in mitochondrial volume in individual cardiomyocyte due to exposure to 30 μM DZ, 10 nM DADLE, 10 μM HOE with or without the F_o-inhibitor VENT. Changes in mitochondrial volume were assessed using a Zeiss 63x/1.4 N.A. oil immersion lens, 633 nm laser illumination, scanning 14.1 pixels/μm along the cell long axis for 72.6 or 145.1 μm). Fourier analysis (ImageJ, W. Rasband, NIH, Bethesda, MD) of repeating intensity of the linescan image provided the long-axis spacing of the sarcomere and mitochondrial compartments (from the 1st and 2nd order spectral peaks, enabling resolution of changes in dimension of ~1% in 1 μm structures). The position of the major Fourier spectral peak corresponding to ~1 μm spatial structures gives the average mitochondrial diameter, and the peak-width gives an index of the variability about the mean (details of this procedure are described in (Juhaszova et al, 2004)).

VO_2 measurements and flavoprotein fluorescence in intact cardiomyocytes

Cell respiration (VO_2) was measured by the Clark-type O_2 electrode based Mitocell S200 micro respirometry system (Strathkelvin Instruments Ltd. North Lanarkshire, UK).

Oxidation of the flavoprotein (FP) pool is known to increase the blue light-excited cellular autofluorescence (Juhaszova et al, 2004; Sato et al, 1998). Endogenous flavoprotein fluorescence was excited by an argon 488 nm laser line (attenuated to 1%) on a Zeiss LSM 510 using a 40x 1.3 NA oil objective. Emitted fluorescence was recorded at LP 505 nm. Relative fluorescence was calibrated to the values measured after 2,4-dinitrophenol (DNP) (fully oxidized) and cyanide exposure (fully reduced). Cells were continuously perfused (1-2 ml/min) and a time series of images was collected at intervals of 20 seconds. After baseline fluorescence was acquired (5 min), cells were exposed to diazoxide (10 min) and the experiment was completed by exposing the cells to DNP. Fluorescence traces from individual cell in the acquisition view were analyzed by MetaMorph image analysis software (Molecular Devices, Sunnyvale, CA) and then averaged.

Results are normalized to the dynamic range achieved in each cell when exposed to DNP, which by producing sufficient respiratory uncoupling, yields the maximum degree of autofluorescence change possible due to FP oxidation.

Mitochondrial swelling, membrane potential and K^+ flux determination in isolated mitochondria

Mitochondria from guinea pig heart were isolated and assayed as described elsewhere (Aon et al, 2010). Briefly, mitochondrial swelling, membrane potential (ΔΨm), and PBFI were monitored simultaneously with a spectrofluorimeter (Photon Technology, Inc.; Edison NJ) in an experimental solution containing (in mM): 250 sucrose (or 137 KCl), 0.5 EGTA, 2.5 $MgCl_2$, 20 HEPES, 2 Pi, pH 7.2. Mitochondrial swelling was measured as a decrease in the 90° light scattering signal using 520 nm excitation. ΔΨm was recorded using 100 nM TMRM and quantified with a ratiometric method (Scaduto & Grotyohann, 1999). PBFI fluorescence was monitored ratiometrically (340/380 nm excitation at 495 nm emission).

Determination of mitochondrial permeability transition threshold

We have previously developed and extensively tested a model enabling the precise determination of the mPTP sensitivity to oxidant stress in intact cardiac myocytes (Juhaszova et al, 2004; Zorov et al, 2000). Briefly, small numbers of mitochondria inside isolated cardiomyocytes were exposed in situ to conditions of oxidative stress by repetitive (2 Hz) laser line-scanning (with imaging) of a single row of mitochondria in a cell loaded with 100 nM tetramethylrhodamine methyl ester (TMRM), using a Zeiss LSM-510 inverted confocal microscope. This results in incremental, additive exposure of only the laser-exposed area to the photodynamic production of ROS and consequent mPTP induction. The ROS-threshold for mPTP induction (t_{MPT}) was measured as the average time necessary to induce the mPTP due to the local buildup of ROS in a row consisting of ~25 mitochondria.

Generation of $IF1^{-/-}$ mice

Mice carrying a genetically inactivated allele at the Atpif1 locus (C57BL/6NTac-Atpif1$^{tm1a(EUCOMM)Wtsi}$/WtsiCnbc), originally generated by the Wellcome Trust Sanger Institute for the EUCOMM project, within the International KnockOut Mouse Consortium (IKMC) (Bradley et al, 2012), were obtained from the Spanish node of the European Mouse Mutant Archive (EMMA, http://www.infrafrontier.eu, mouse strain EM:05233) at the National Centre for Biotechnology in Madrid (Spain) and bred to homozygosity. Resulting homozygous mice are referred to as $IF_1^{-/-}$ in this manuscript. Mice were genotyped through a combination of separate PCR reactions that detect LacZ, the gene-specific wild type allele, and a mutant allele-specific short range PCR. For the phenotype verification of IF_1 KO mouse see Figure 5D-figure supplement 1.

PCRs primer pairs and expected size bands:

PCR type	Forward primer	Reverse primer	Expected size (bp)
Mutant PCR	Atpif1_46360_F	CAS_R1_Term x	114
Wild type PCR	Atpif1_46360_F	Atpif1_46360_R	396
LacZ PCR	LacZ_2_small_F	LacZ_2_small_R	108

Primer sequences:

Primer names:	Primer sequence (5' > 3')
CAS_R1_Term	TCGTGGTATCGTTATGCGCC
Atpif1_46360_F	TGCCTGACATTGGTATTGGG
Atpif1_46360_R	GTGCAGCTTGTGGGAGTCAG
LacZ_2_small_F	ATCACGACGCGCTGTATC
LacZ_2_small_R	ACATCGGGCAAATAATATCG

IF_1 gene silencing by RNA interference

Neonatal cardiac myocytes were isolated from 1- to 3-day-old Wistar rats by enzymatic digestion (Chesley et al, 2000) and cultured for two days before transfection with a pool of four short interfering RNAs (siRNAs; 100 nM) targeted specifically to IF_1 using GeneSilencer reagent (Gene Therapy Systems Inc., San Diego, California, USA) according to the protocol provided by the company. Four siRNA duplexes were designed and synthesized by Dharmacon Inc. (Lafayette, Colorado, USA) to target the rat IF_1: (a) 5'-AAACAGATCGAACGGCATA-3'; (b) 5'-AAAGAATAGTGAGCATTGA-3'; (c) 5 '-GGAGATAGAGCGTCTGCAA-3'; (d) 5'-CGTATGAGGGTCCTGCAAA-3'. As a negative control, cells were transfected with siRNA against GFP (Dharmacon Inc.). Experiments were performed 72 hours after transfection.

Phylogenetic tree of the BH3 extended peptides

The IF_1 peptide BH3 motif appears to have diverged from the evolutionary branch originating BID and BIK Bcl-2 family members. The analysis of a 35 residue fragment from IF_1 ranging from fungi to human aligned together with 79 fragments containing BH3 motifs with similarities to the 26 residue BAD peptide used in our functional studies (Figure 8-figure supplement 1) leads to the tree shown in Figure 8-figure supplement 3. MEGA enabled the calculation of the divergence time of $1690{\times}10^6$ years when IF_1 ancestor proteins separated from the ones that would originate BID, BIK and Bcl-2-like protein 13. The tree obtained from the Clustal Omega alignment (Figure 8-figure supplement 2) shows largely the same group division that has been considered elsewhere (Aouacheria et al, 2013). In spite of our analysis being limited to only a fragment containing the BH3 motif, the same groups were obtained, i.e., BID-like, Bcl-2-like, also containing Bcl-xL (Lanave et al, 2004), and a Bax-like (Aouacheria et al, 2013). Additionally, an independent assessment of the alignment and phylogenetic analysis was performed with the program BAli-Phy (Figure 8-figure supplement 3). This rendered essentially a similar tree which mainly differed from the tree in Figure 8-figure supplement 2 regarding the relative position of the Beclin and BAX groups (Figure 8-figure supplement 3). In our case there was no drift in the evolution of the hidden Markov Model (HMM) and the analysis of several Markov Chain Monte Carlo (MCMC) runs demonstrated convergence of the various chains toward a consensus alignment and phylogenetic tree. The main difference with the HMM described by Aouacheria (Aouacheria et al, 2013) is that longer fragments containing the so-called affinity enhancing motifs flanking the BH3 motif (Yang, 2010) were considered in the present work which renders the alignment more stringent.

Phylogenetic tree of the BH3 extended peptides

Sequence Alignment and tree computation methods

The sequences aligned were obtained from the UniProt website (EMBL-EBI; http://www.uniprot.org). First, the BH3-containing proteins were obtained by performing a BLAST search of the BAD peptide (26 AA peptide used in our functional studies). A collection of 79 sequences of BH3 containing proteins was retrieved expanding from yeast to mammals including proteins from the BAD, BAK, BAX, BID, BIK, PUMA, MCL-1 and BECLIN groups. Then, a collection of 28 IF1 sequences, mostly manually annotated and reviewed, was gathered and aligned using Clustal Omega (http://www.clustal.org/omega). The fragments of the sequences obtained by this alignment were saved and used for subsequent analysis. These fragments correspond to 35 amino acids that contain the pattern of the original BAD peptide that was used as the seed. The unaligned peptides were used as input sequences for BAli-Phy (v 2.3.6 (Redelings & Suchard, 2005)) a Linux program that uses Bayesian estimation and Markov Chain Monte Carlo (MCMC) methods to sample from the posterior distribution of alignments. Both alignments obtained from Clustal Omega and from BAli-Phy were utilized to construct the respective phylogenetic trees using the program MEGA 6.0 (Tamura et al, 2013) which allows computation of the the distances and the evolutionary times after linearization of the distances of divergence. For those calculations the reference point for the divergence between man and an ascomycete was $1540\times10^6 \pm 250 \times10^6$ years (1540 Myr). The calculation of the tree was performed with the Neighbor Joining method (Saitou & Nei, 1987).

Statistics

All experiments were performed at least in triplicate, with cell number greater than 12 in each independent experiment unless stated otherwise. All data are mean ± SEM. Comparisons within groups were made by an appropriate one-way ANOVA or Student t test, and P value <0.05 was considered as statistically significant.

Author contributions

Conceptualization, M.J., D.B.Z. and S.J.S.; Methodology, M.J., E.K., H.B.N., K.W.F., L.M., M.A.A., S.C. and S.J.S.; Software, Y.Y., S.B.G. and S.C.; Formal Analysis, Y.Y., S.B.G., S.C. and S.J.S.; Investigation, M.J., E.K., D.B.Z., H.B.N., M.A.A. and S.C.; Resources, R.dC., L.M., S.B.G. and S.J.S.; Writing-Original Draft, S.J.S.; Writing-Review & Editing, M.J., E.K., D.B.Z., K.W.F., R.dC., S.B.G., M.A.A., S.C. and S.J.S.; Visualization, M.J., E.K., Y.Y., S.B.G., M.A.A., S.C. and S.J.S.; Supervision, S.J.S.

Acknowledgments

We thank E.G. Lakatta for useful discussions, D. Boyer for animal husbandry, L. Rezanka for mice genotyping and M.J. del Hierro Sanchez for assistance in obtaining the transgenic $IF_1^{-/-}$ mice. This work was supported entirely by the Intramural Research Program, National Institute on Aging, NIH.

Conflict of interest

The authors declare that they have no conflict of interest.

References

Abrahams JP, Leslie AG, Lutter R, Walker JE (1994) Structure at 2.8 A resolution of F1-ATPase from bovine heart mitochondria. *Nature* **370:** 621-628

Alavian KN, Li H, Collis L, Bonanni L, Zeng L, Sacchetti S, Lazrove E, Nabili P, Flaherty B, Graham M, Chen Y, Messerli SM, Mariggio MA, Rahner C, McNay E, Shore GC, Smith PJ, Hardwick JM, Jonas EA (2011) Bcl-xL regulates metabolic efficiency of neurons through interaction with the mitochondrial F1FO ATP synthase. *Nat Cell Biol* **13:** 1224-1233

Antos CL, McKinsey TA, Frey N, Kutschke W, McAnally J, Shelton JM, Richardson JA, Hill JA, Olson EN (2002) Activated glycogen synthase-3 beta suppresses cardiac hypertrophy in vivo. *Proc Natl Acad Sci U S A* **99:** 907-912

Aon MA, Cortassa S, Wei AC, Grunnet M, O'Rourke B (2010) Energetic performance is improved by specific activation of K+ fluxes through K(Ca) channels in heart mitochondria. *Biochim Biophys Acta* **1797:** 71-80

Aouacheria A, Rech de Laval V, Combet C, Hardwick JM (2013) Evolution of Bcl-2 homology motifs: homology versus homoplasy. *Trends Cell Biol* **23:** 103-111

Bason JV, Montgomery MG, Leslie AG, Walker JE (2014) Pathway of binding of the intrinsically disordered mitochondrial inhibitor protein to F1-ATPase. *Proc Natl Acad Sci U S A* **111:** 11305-11310

Bednarczyk P, Dolowy K, Szewczyk A (2005) Matrix Mg2+ regulates mitochondrial ATP-dependent potassium channel from heart. *FEBS Lett* **579:** 1625-1632

Boyer PD (1997) The ATP synthase--a splendid molecular machine. *Annu Rev Biochem* **66:** 717-749

Bradley A, Anastassiadis K, Ayadi A, Battey JF, Bell C, Birling MC, Bottomley J, Brown SD, Burger A, Bult CJ, Bushell W, Collins FS, Desaintes C, Doe B, Economides A, Eppig JT, Finnell RH, Fletcher C, Fray M, Frendewey D, Friedel RH, Grosveld FG, Hansen J, Herault Y, Hicks G, Horlein A, Houghton R, Hrabe de Angelis M, Huylebroeck D, Iyer V, de Jong PJ, Kadin JA, Kaloff C, Kennedy K, Koutsourakis M, Lloyd KC, Marschall S, Mason J, McKerlie C, McLeod MP, von Melchner H, Moore M, Mujica AO, Nagy A, Nefedov M, Nutter LM, Pavlovic G, Peterson JL, Pollock J, Ramirez-Solis R, Rancourt DE, Raspa M, Remacle JE, Ringwald M, Rosen B, Rosenthal N, Rossant J, Ruiz Noppinger P, Ryder E, Schick JZ, Schnutgen F, Schofield P, Seisenberger C, Selloum M, Simpson EM, Skarnes WC, Smedley D, Stanford WL, Stewart AF, Stone K, Swan K, Tadepally H, Teboul L, Tocchini-Valentini GP, Valenzuela D, West AP, Yamamura K, Yoshinaga Y, Wurst W (2012) The mammalian gene function resource: the International Knockout Mouse Consortium. *Mamm Genome* **23:** 580-586

Campanella M, Casswell E, Chong S, Farah Z, Wieckowski MR, Abramov AY, Tinker A, Duchen MR (2008) Regulation of mitochondrial structure and function by the F1Fo-ATPase inhibitor protein, IF1. *Cell Metab* **8:** 13-25

Capogrossi MC, Kort AA, Spurgeon HA, Lakatta EG (1986) Single adult rabbit and rat cardiac myocytes retain the Ca2+- and species-dependent systolic and diastolic contractile properties of intact muscle. *J Gen Physiol* **88:** 589-613

Chesley A, Lundberg MS, Asai T, Xiao RP, Ohtani S, Lakatta EG, Crow MT (2000) The beta(2)-adrenergic receptor delivers an antiapoptotic signal to cardiac myocytes through G(i)-dependent coupling to phosphatidylinositol 3'-kinase. *Circ Res* **87:** 1172-1179

Contessi S, Metelli G, Mavelli I, Lippe G (2004) Diazoxide affects the IF1 inhibitor protein binding to F1 sector of beef heart F0F1ATPsynthase. *Biochem Pharmacol* **67:** 1843-1851

Cross RL, Muller V (2004) The evolution of A-, F-, and V-type ATP synthases and ATPases: reversals in function and changes in the H+/ATP coupling ratio. *FEBS Lett* **576:** 1-4

Dahlem YA, Horn TF, Buntinas L, Gonoi T, Wolf G, Siemen D (2004) The human mitochondrial KATP channel is modulated by calcium and nitric oxide: a patch-clamp approach. *BiochimBiophysActa* **1656:** 46-56

Feniouk BA, Kozlova MA, Knorre DA, Cherepanov DA, Mulkidjanian AY, Junge W (2004) The proton-driven rotor of ATP synthase: ohmic conductance (10 fS), and absence of voltage gating. *Biophys J* **86:** 4094-4109

Follis AV, Chipuk JE, Fisher JC, Yun MK, Grace CR, Nourse A, Baran K, Ou L, Min L, White SW, Green DR, Kriwacki RW (2013) PUMA binding induces partial unfolding within BCL-xL to disrupt p53 binding and promote apoptosis. *Nature chemical biology* **9:** 163-168

Formentini L, Pereira MP, Sanchez-Cenizo L, Santacatterina F, Lucas JJ, Navarro C, Martinez-Serrano A, Cuezva JM (2014) In vivo inhibition of the mitochondrial H+-ATP synthase in neurons promotes metabolic preconditioning. *EMBO J* **33:** 762-778

Formentini L, Sanchez-Arago M, Sanchez-Cenizo L, Cuezva JM (2012) The mitochondrial ATPase inhibitory factor 1 triggers a ROS-mediated retrograde prosurvival and proliferative response. *Mol Cell* **45:** 731-742

Foster DB, Ho AS, Rucker J, Garlid AO, Chen L, Sidor A, Garlid KD, O'Rourke B (2012) Mitochondrial ROMK channel is a molecular component of mitoK(ATP). *Circ Res* **111:** 446-454

Garlid KD, Dos Santos P, Xie ZJ, Costa AD, Paucek P (2003) Mitochondrial potassium transport: the role of the mitochondrial ATP-sensitive K(+) channel in cardiac function and cardioprotection. *Biochim Biophys Acta* **1606:** 1-21

Geer LY, Domrachev M, Lipman DJ, Bryant SH (2002) CDART: protein homology by domain architecture. *Genome Res* **12:** 1619-1623

Giorgio V, von Stockum S, Antoniel M, Fabbro A, Fogolari F, Forte M, Glick GD, Petronilli V, Zoratti M, Szabo I, Lippe G, Bernardi P (2013) Dimers of mitochondrial ATP synthase form the permeability transition pore. *Proc Natl Acad Sci U S A* **110:** 5887-5892

Gledhill JR, Montgomery MG, Leslie AG, Walker JE (2007) How the regulatory protein, IF(1), inhibits F(1)-ATPase from bovine mitochondria. *Proc Natl Acad Sci U S A* **104:** 15671-15676

Grigoriev SM, Skarga YY, Mironova GD, Marinov BS (1999) Regulation of mitochondrial KATP channel by redox agents. *Biochim Biophys Acta* **1410:** 91-96

Halestrap AP (1989) The regulation of the matrix volume of mammalian mitochondria in vivo and in vitro and its role in the control of mitochondrial metabolism. *Biochim Biophys Acta* **973:** 355-382

Hille B (2001) *Ion Channels of Excitable Membranes*, 3rd edn.: Sinauer Associates, Inc.

Jiang MT, Ljubkovic M, Nakae Y, Shi Y, Kwok WM, Stowe DF, Bosnjak ZJ (2006) Characterization of human cardiac mitochondrial ATP-sensitive potassium channel and its regulation by phorbol ester in vitro. *AmJPhysiol Heart CircPhysiol* **290:** H1770-H1776

Juhaszova M, Wang S, Zorov DB, Nuss HB, Gleichmann M, Mattson MP, Sollott SJ (2008) The identity and regulation of the mitochondrial permeability transition pore: where the known meets the unknown. *Ann N Y Acad Sci* **1123:** 197-212

Juhaszova M, Zorov DB, Kim SH, Pepe S, Fu Q, Fishbein KW, Ziman BD, Wang S, Ytrehus K, Antos CL, Olson EN, Sollott SJ (2004) Glycogen synthase kinase-3beta mediates convergence of protection signaling to inhibit the mitochondrial permeability transition pore. *J Clin Invest* **113:** 1535-1549

Juhaszova M, Zorov DB, Yaniv Y, Nuss HB, Wang S, Sollott SJ (2009) Role of glycogen synthase kinase-3beta in cardioprotection. *Circ Res* **104:** 1240-1252

Kaim G, Dimroth P (1995) A double mutation in subunit c of the Na(+)-specific F1F0-ATPase of Propionigenium modestum results in a switch from Na+ to H(+)-coupled ATP synthesis in the Escherichia coli host cells. *J Mol Biol* **253:** 726-738

Kaim G, Wehrle F, Gerike U, Dimroth P (1997) Molecular basis for the coupling ion selectivity of F1F0 ATP synthases: probing the liganding groups for Na+ and Li+ in the c subunit of the ATP synthase from Propionigenium modestum. *Biochemistry* **36:** 9185-9194

Kelekar A, Chang BS, Harlan JE, Fesik SW, Thompson CB (1997) Bad is a BH3 domain-containing protein that forms an inactivating dimer with Bcl-XL. *Mol Cell Biol* **17:** 7040-7046

Korge P, Honda HM, Weiss JN (2005) K+-dependent regulation of matrix volume improves mitochondrial function under conditions mimicking ischemia-reperfusion. *Am J Physiol Heart Circ Physiol* **289:** H66-77

Kuhlbrandt W, Davies KM (2016) Rotary ATPases: A New Twist to an Ancient Machine. *Trends Biochem Sci* **41:** 106-116

Lanave C, Santamaria M, Saccone C (2004) Comparative genomics: the evolutionary history of the Bcl-2 family. *Gene* **333:** 71-79

Leone V, Pogoryelov D, Meier T, Faraldo-Gomez JD (2015) On the principle of ion selectivity in Na+/H+-coupled membrane proteins: experimental and theoretical studies of an ATP synthase rotor. *Proc Natl Acad Sci U S A* **112:** E1057-1066

Miedema H, van Walraven HS, de Boer AH (1994) Potassium selective and venturicidin sensitive conductances of Fo purified from bovine heart mitochondria, reconstituted in planar lipid bilayers. *Biochem Biophys Res Commun* **203:** 1005-1012

Mironova GD, Fedotcheva NI, Makarov PR, Pronevich LA, Mironov GP (1981) [Protein from beef heart mitochondria inducing the potassium channel conductivity of bilayer lipid membrane]. *Biofizika* **26:** 451-457

Mironova GD, Negoda AE, Marinov BS, Paucek P, Costa AD, Grigoriev SM, Skarga YY, Garlid KD (2004) Functional distinctions between the mitochondrial ATP-dependent K+ channel (mitoKATP) and its inward rectifier subunit (mitoKIR). *J Biol Chem* **279:** 32562-32568

Mironova GD, Skarga YY, Grigoriev SM, Negoda AE, Kolomytkin OV, Marinov BS (1999) Reconstitution of the mitochondrial ATP-dependent potassium channel into bilayer lipid membrane. *J Bioenerg Biomembr* **31:** 159-163

Mitchell P (1961) Coupling of phosphorylation to electron and hydrogen transfer by a chemi-osmotic type of mechanism. *Nature* **191:** 144-148

Nakae Y, Kwok WM, Bosnjak ZJ, Jiang MT (2003) Isoflurane activates rat mitochondrial ATP-sensitive K+ channels reconstituted in lipid bilayers. *AmJPhysiol Heart CircPhysiol* **284:** H1865-H1871

Nicholls DG, Ferguson SJ (2013) *Bioenergetics4*: Academic Press.

Noji H, Yasuda R, Yoshida M, Kinosita K, Jr. (1997) Direct observation of the rotation of F1-ATPase. *Nature* **386:** 299-302

O'Neill JW, Manion MK, Maguire B, Hockenbery DM (2006) BCL-XL dimerization by three-dimensional domain swapping. *J Mol Biol* **356:** 367-381

Paucek P, Mironova G, Mahdi F, Beavis AD, Woldegiorgis G, Garlid KD (1992) Reconstitution and partial purification of the glibenclamide-sensitive, ATP-dependent K+ channel from rat liver and beef heart mitochondria. *J Biol Chem* **267:** 26062-26069

Petros AM, Medek A, Nettesheim DG, Kim DH, Yoon HS, Swift K, Matayoshi ED, Oltersdorf T, Fesik SW (2001) Solution structure of the antiapoptotic protein bcl-2. *Proc Natl Acad Sci U S A* **98:** 3012-3017

Rajan S, Choi M, Nguyen QT, Ye H, Liu W, Toh HT, Kang C, Kamariah N, Li C, Huang H, White C, Baek K, Gruber G, Yoon HS (2015) Structural transition in Bcl-xL and its potential association with mitochondrial calcium ion transport. *Sci Rep* **5:** 10609

Redelings BD, Suchard MA (2005) Joint Bayesian estimation of alignment and phylogeny. *Syst Biol* **54:** 401-418

Saitou N, Nei M (1987) The neighbor-joining method: a new method for reconstructing phylogenetic trees. *Mol Biol Evol* **4:** 406-425

Sato T, O'Rourke B, Marban E (1998) Modulation of mitochondrial ATP-dependent K+ channels by protein kinase C. *Circ Res* **83:** 110-114

Scaduto RC, Jr., Grotyohann LW (1999) Measurement of mitochondrial membrane potential using fluorescent rhodamine derivatives. *Biophys J* **76:** 469-477

Sievers F, Wilm A, Dineen D, Gibson TJ, Karplus K, Li W, Lopez R, McWilliam H, Remmert M, Soding J, Thompson JD, Higgins DG (2011) Fast, scalable generation of high-quality protein multiple sequence alignments using Clustal Omega. *Mol Syst Biol* **7:** 539

Stock D, Leslie AG, Walker JE (1999) Molecular architecture of the rotary motor in ATP synthase. *Science* **286:** 1700-1705

Strauss M, Hofhaus G, Schroder RR, Kuhlbrandt W (2008) Dimer ribbons of ATP synthase shape the inner mitochondrial membrane. *EMBO J* **27:** 1154-1160

Tamura K, Stecher G, Peterson D, Filipski A, Kumar S (2013) MEGA6: Molecular Evolutionary Genetics Analysis version 6.0. *Mol Biol Evol* **30:** 2725-2729

van Raaij MJ, Orriss GL, Montgomery MG, Runswick MJ, Fearnley IM, Skehel JM, Walker JE (1996) The ATPase inhibitor protein from bovine heart mitochondria: the minimal inhibitory sequence. *Biochemistry* **35:** 15618-15625

Walker JE (1994) The regulation of catalysis in ATP synthase. *Current opinion in structural biology* **4:** 912-918

Wang JL, Zhang ZJ, Choksi S, Shan S, Lu Z, Croce CM, Alnemri ES, Korngold R, Huang Z (2000) Cell permeable Bcl-2 binding peptides: a chemical approach to apoptosis induction in tumor cells. *Cancer Res* **60:** 1498-1502

Wittig I, Carrozzo R, Santorelli FM, Schagger H (2006) Supercomplexes and subcomplexes of mitochondrial oxidative phosphorylation. *Biochim Biophys Acta* **1757:** 1066-1072

Xu W, Liu Y, Wang S, McDonald T, Van Eyk JE, Sidor A, O'Rourke B (2002) Cytoprotective role of Ca2+- activated K+ channels in the cardiac inner mitochondrial membrane. *Science* **298:** 1029-1033

Yang J (2010) Molecular modeling of human BAD, a pro-apoptotic Bcl-2 family member, integrating glycolysis and apoptosis. *Protein Pept Lett* **17:** 206-220

Zhang DX, Chen YF, Campbell WB, Zou AP, Gross GJ, Li PL (2001) Characteristics and superoxide-induced activation of reconstituted myocardial mitochondrial ATP-sensitive potassium channels. *CircRes* **89:** 1177-1183

Zorov DB, Filburn CR, Klotz LO, Zweier JL, Sollott SJ (2000) Reactive oxygen species (ROS)-induced ROS release: a new phenomenon accompanying induction of the mitochondrial permeability transition in cardiac myocytes. *J Exp Med* **192:** 1001-1014

Zorov DB, Juhaszova M, Sollott SJ (2014) Mitochondrial reactive oxygen species (ROS) and ROS-induced ROS release. *Physiol Rev* **94:** 909-950

Zorov DB, Juhaszova M, Yaniv Y, Nuss HB, Wang S, Sollott SJ (2009) Regulation and pharmacology of the mitochondrial permeability transition pore. *Cardiovasc Res* **83:** 213-225

Zotova L, Aleschko M, Sponder G, Baumgartner R, Reipert S, Prinz M, Schweyen RJ, Nowikovsky K (2010) Novel components of an active mitochondrial K(+)/H(+) exchange. *J Biol Chem* **285:** 14399-14414